Chronology of formation of early solar system solids from bulk Mg isotope analyses of CV3 chondrules

Hsin-Wei Chen[1], Jennifer L. Claydon[2], Tim Elliott[1], Christopher D. Coath[1], Yi-Jen Lai[1,2,3] and Sara S. Russell[2]

[1] Bristol Isotope Group, School of Earth Sciences, University of Bristol, Bristol, BS8 1RJ, UK

[2]Natural History Museum, Meteoritic and Cosmic Mineralogy, Cromwell Road, SW7 5BD, London, UK

[3]Institute of Geochemistry and Petrology, ETH Zürich, Zürich, Switzerland

Abstract

We have analysed the petrography, major element abundances and bulk Al-Mg isotope systematics of 19 ferromagnesian chondrules from the CV3 chondrites Allende, Mokoia, and Vigarano, together with an Al-rich chondrule and refractory olivine from Mokoia. Co-variations of Al/Mg with Na/Mg and Ti/Mg in our bulk chondrules suggest their compositions are dominantly controlled by reworking of different proportions of chondrule components (e.g. mafic minerals and mesostatis); their precursors are thus fragments from prior generations of chondrules. Our samples show a range in fractionation corrected $^{26}Mg/^{24}Mg$ ($\Delta'^{26}Mg$) ~60ppm, relative to precisions <±5ppm (2se) and these values broadly covary with $^{27}Al/^{24}Mg$. The data can be used to calculate model initial $^{26}Al/^{27}Al$, or $(^{26}Al/^{27}Al)_0$, of the chondrule precursors. Our resolvably radiogenic chondrules yield model $(^{26}Al/^{27}Al)_0$ ~1-2x10^{-5}, equivalent to model "ages" of precursor formation □ 1Ma post CAI. However, many of our chondrules show near solar $\Delta'^{26}Mg$ and no variability despite a range in $^{27}Al/^{24}Mg$. This suggests their derivation either from younger precursor chondrules or open system behaviour once ^{26}Al was effectively extinct ($(^{26}Al/^{27}Al)_0$<0.8x10^{-5}, given the resolution here). Evidence for the latter explanation is provided by marked rims of orthopyroxene replacing olivine, indicating reaction of chondrules with a surrounding silicate vapour. Concurrent isotopic exchange of Mg with a near chondritic vapour during late reworking could explain their isotopic systematics. One ferromagnesian object is dominated by a high Mg# olivine with elevated Ti and Ca abundances. This refractory olivine has a markedly negative $\Delta'^{26}Mg$ = -16±3 ppm (2se), reflecting its early removal (model age of <0.5Ma post CAI), from a reservoir with evolving $\Delta'^{26}Mg$. If representative of the chondrule forming region, this grain defines a minimum interval of radiogenic ingrowth for CV chondrites commensurate with $(^{26}Al/^{27}Al)_0$>3.4±0.6x10^{-5}. Overall, our samples record a sequence of events from the formation of ferromagnesian objects within 0.5Ma of CAI to re-equilibration of chondrules and

silicate vapour >2Ma post CAI, assuming an initially homogeneous $^{26}Al/^{27}Al$. Metamorphism on the asteroid parent body may have played a subsequent role in affecting Mg isotope composition, but we argue this had a minor influence on the observations here.

1 Introduction

Chondrules, the eponymous main constituent of most primitive meteorites, carry a unique record of processes occurring in the early solar system, but interpreting the information contained within these quenched melt droplets is challenging. Critical to this aim is establishing a timescale for the events that shaped their evolution. It is possible to apply both extant U-Pb and extinct Al-Mg isotopic systems to yield high precision ages of chondrules, but each poses different problems. A robust chronology clearly requires consistent ages to be derived from both approaches. Currently, this is not obviously the case, since the ages of some chondrules determined by internal Pb-Pb isochrons (CONNELLY et al., 2012; BOLLARD et al 2017) are as old as the oldest solar system solids (calcium aluminium rich inclusions or CAIs), whereas internal Al-Mg isochrons are apparently systematically younger than CAI by >1Ma (e.g. KITA AND USHIKUBO, 2012).

One obvious explanation of this disparity is that Al-Mg chronology requires an assumption of $^{26}Al/^{27}Al$ homogeneity in the solar nebula, which has long been questioned (e.g. SHU et al., 1996). The debate has been reinvigorated with new perspectives provided by high precision Mg isotope work on bulk chondrites (e.g. KITA et al., 2013; LARSEN et al., 2011; WASSERBURG et al., 2012), CAIs (e.g. WASSERBURG et al., 2012) and achondrites (SCHILLER et al., 2015). The coupled issues of chronology and the distribution of ^{26}Al in the early solar system can be further explored by studying bulk Mg isotope compositions of individual chondrules. The Mg isotope composition of a bulk chondrule provides usefully different chronological constraints compared to more traditional internal isochrons (see KITA AND USHIKUBO, 2012), as it depends on the timing of Al/Mg fractionation in chondrule precursors, rather than chondrule crystallisation. A purely chronological reconciliation of Pb-Pb and Al-Mg ages might be possible if bulk Al-Mg analyses record older model ages than those of mineral Al-Mg isochrons. In this hypothetical situation, the former could reflect formation of precursors in more ancient events, recorded by some Pb-Pb analyses, whereas the latter could have been reset by subsequent heating episodes.

The range in Al/Mg found in bulk chondrules, however, is much more restricted than between phases used for *in situ* analysis, and their low bulk Al/Mg means the contribution of radiogenic Mg is smaller. Thus more precise Mg isotope measurements are required to realise this potential. Multi-collector inductively-coupled mass-spectrometry (MC-ICPMS) has made this approach analytically tractable and precisions of <5ppm are now possible (BIZZARRO et al., 2011).

Initial bulk chondrule Al-Mg analyses from Allende implied $(^{26}Al/^{27}Al)_0$ as high as CAI, ~$5x10^{-5}$ (GALY et al., 2000, BIZZARRO et al., 2004) in their precursors, in keeping with model scenario outlined above. In contrast, a later coupled study of *in situ* and bulk chondrule analyses on the same meteorite yielded less radiogenic values and consistent $(^{26}Al/^{27}Al)_0$ between *in situ* and bulk approaches (LUU et al., 2015). Further studies have expanded the number chondrite groups studied (BOUVIER et al., 2013, GOUNELLE et al., 2007) and reported data at improved precision (OLSEN et al., 2013, VAN KOOTEN et al., 2015, OLSEN et al., 2016). Higher precision allows possible resolution of Mg isotopic variations in more typical, lower Al chondrules. Yet for chondrules of a given chondrite group, these recent studies report only minor variation (<10ppm) in fractionation corrected $^{26}Mg/^{24}Mg$ ($\Delta'^{26}Mg$), despite variable $^{27}Al/^{24}Mg$, implying low $(^{26}Al/^{27}Al)_0$ (<$1x10^{-5}$) in the chondrule precursors. We further explore these seemingly divergent results with high precision bulk chondrule analyses from a previously unstudied, oxidised CV3 chondrite (Mokoia) in addition to new data from two CV3 chondrites (Vigarano and Allende) for which published bulk Al-Mg systematics are strikingly different (BIZZARRO et al., 2004, LUU et al., 2015, OLSEN et al., 2016).

2 Analytical Techniques

Chips of CV3 meteorites Allende (CVoxA; BM 1969, 148), Mokoia (BM 1910, 729) and Vigarano (CVred; BM1920, 347) were provided by the Natural History Museum (NHM), London. The chips were gently crushed using an agate pestle and mortar to release chondrules from the matrix. The compact matrix of Vigarano meant that gentle crushing alone did not release the chondrules, so the chip was also agitated in a glass vial. Any remaining matrix material was removed by scraping using ceramic tweezers. Chondrules (showing rounded edges) with masses > 0.25 mg were selected and split into two or more fragments using an agate pestle and mortar. One fragment of each chondrule was mounted in a resin block and polished using diamond paste and the

remainder saved for chemical analysis. The fragments for chemical analysis were checked in an optical microscope to ensure they appeared to be representative of the bulk chondrule.

We obtained back-scattered electron (BSE) images and X-ray element maps of each chondrule fragment using the Zeiss EVO 15LS Scanning Electron Microscope at the NHM at an operating potential of 20 kV and working distance of 8.5 mm. Mineral compositions were determined using the Cameca SX100 Electron Microprobe at the NHM using a beam current of 20 nA at 20 kV and appropriate mineral standards. The electron beam was defocused from 2 µm to 10 µm when measuring plagioclase compositions, in order to minimise loss of sodium.

All wet chemistry was carried out in the HEPA filtered clean laboratory of the Bristol Isotope Group, University of Bristol. Chondrule fragments were cleaned by ultrasonification in 18 MΩcm H_2O for ten minutes, followed by ultrasonification in acetone for five minutes. This cleaning step was repeated three times. The fragments were then weighed (Table 1) before being dissolved by refluxing in 200 µl of an HF-HNO_3 acid mixture at 130 °C. After drying down, 1 ml 6M HCl was added and samples heated to 130 °C to attain complete dissolution. The chondrules were prepared and analysed in three separate batches, as indicated in Table 1. Aliquots of powder from reference rock materials and blanks were also prepared using the same procedures.

After initial dissolution, each sample was re-dissolved in 2% HNO_3 and 20% by volume removed and made up to 5 ml in 2M HNO_3. The relative abundances of Al, Mg, Fe, Ni, Na and Ti were determined on these aliquots using a quadrupole ICP-MS (Agilent 7700x) at the NHM. The instrument was calibrated using either single element standards (Alfa Aesar Ltd.) or mixed standards (CCS-4, CCS-5, CCS-6; Inorganic Ventures Inc.). Typically 6-8 standards were used for each element with concentrations ranging from 1 to 1000 µg l^{-1} (10,000 µg L^{-1} for Mg, Al and Fe). To minimise polyatomic interferences, the instrument was run with 5 ml min^{-1} He (99.9995% purity) in the collision-reaction octopole cell (CRC), as well as with no collision gas entering the CRC. ^{23}Na was determined in the 'no gas' mode while all other elements were determined in the 'He mode'. Insignificant differences between the results obtained in either mode suggests that the polyatomic interferences were negligible. An internal standard (^{103}Rh) was introduced in-line via a t-piece. Drift was monitored by analysing a mixed standard (10 µg l^{-1}) after every 10 samples.

We did not attempt to quantify absolute elemental abundances, given the inaccuracies in weighing ~1mg of sample on the available balance with nominal 0.01mg resolution and so we only report elemental data as ratios (Table 1). Repeat Al/Mg measurements for aliquots of the same sample run in the same batch reproduce better than 1%. Separate dissolutions of JP-1 associated with sample batches 2 and 3 were run as unknowns and their measured Al/Mg varied by 5% and -2% relative to the value reported by Imai et al. (1995), see Table 1. The peridotite standard JP-1 has a lower Al abundance than the chondrules and so these measurements provide a conservative estimate of the uncertainty of Al/Mg measurements on the chondrules, which we thus ascribe to be ±5%. We report elemental ratios as weight ratios apart from Al/Mg (Table 1), which is expressed as an atomic isotope ratio ($^{27}Al/^{24}Mg$) given it is used as such for chronology.

Magnesium was separated from the remaining 80 vol. % of each sample by using a two-step 2M HNO_3-based cation resin (AG50x12) exchange column described in POGGE VON STRANDMANN (2008) and POGGE VON STRANDMANN et al. (2011). We further removed Mn and Ni from the Mg fraction, collected from the procedure above, both to yield higher a purity Mg solution for analysis and to obtain a Ni separate for isotopic measurement at a later date. This additional separation was achieved on a third, 150µl column of cationic resin (AG50x12) using a mixed 0.55NHCl:95%(v/v) acetone eluent following the approach of VICTOR (1986). Loading and elution of Mn was achieved in 1.5ml of 0.55N HCl:95%(v/v) acetone, the Ni fraction was collected in 1ml of 0.55N HCl:95%(v/v) acetone containing dissolved dimethylglyoxime at 0.1N concentration and Mg was finally collected in 3ml 6N HCl. After each column separation, the Mg fractions were refluxed with H_2O_2 and HNO_3 to destroy any organics released from the resin. Half column volume fractions of eluent before and after the Mg fraction were routinely collected for the first two columns to ensure no Mg was lost, as imperfect yields can lead to mass-dependent fractionation (e.g. TENG et al., 2007). Complete recovery was documented in all samples. We could not similarly monitor the final column chemistry, as the fraction prior to Mg elution comprised the Ni fraction. After making our Mg analyses, we discovered that for three samples significant amounts of Mg were in this preceding Ni fraction. We have subsequently determined these fractional Mg losses and illustrate below that this problem does not impact on our findings.

Mg isotope ratios were measured on a Thermo Finnigan Neptune MC-ICP-MS (s/n 1002) at the University of Bristol. Samples were diluted to be within 5% of a 2.5ppm bracketing DSM3 solution (GALY et al., 2003). Solutions were aspirated with a nominal 50µl/min nebuliser and an Apex Q desolvator. Two combinations of

interface cones were used during this study; 'normal' sample and 'X' skimmer or 'jet' sample and 'H' skimmer. Both gave comparable sensitivities but the latter gave greater mass bias stability and was adopted for the majority of the study. Samples were run using a 'medium' resolution entrance slit (which yields M/ΔM~4000 for 5-95% peak height) in order to enhance signal to noise relative to the strongly, isotopically fractionated Mg instrumental blank. Under the conditions described above, we usually obtained 2nA ^{24}Mg. We simultaneously collected ^{24}Mg, ^{25}Mg and ^{26}Mg in L4, central and H4 faraday cups respectively (the former attached to feedback amplifier with 10^{10} ohm resistor, the others to amplifiers with 10^{11} ohm resistors). We initially set the collection positions to measure ^{26}Mg on the low mass side of the resolved $^{12}C^{14}N^{+}$ interference. We later determined that for our instrumental set-up using H-cones there was no detectable $^{12}C^{14}N^{+}$ contribution (< 2ppm) and so for convenience we measured in the centre of the Mg peaks using a standard centring routine.

The majority of samples were run in a sequence of 120 secs wash, followed by 40x4.2sec measurements of an instrumental on-peak blank and 40x4.2secs of sample or standard, but for a period in the middle of this study (measuring batch 2 and 3 samples with normal sample and x-skimmer cones), the integration times of sample and on-peak blank were increased to 80x4.2secs. The on-peak background measured before each sample and standard was used as the instrumental blank. Sample measurements were bracketed with comparable analyses of the DSM-3 reference. In an analysis session each sample is typically measured in this way 5 times. Normally no data are rejected, and rejection only occurs after manual examination of anomalous interquartile variations, if external factors can reasonably account for the variability (e.g. solution running out).

Reported $\delta^{25}Mg$ are the relative differences of the blank subtracted $^{25}Mg/^{24}Mg$ of the samples and the mean, blank subtracted $^{25}Mg/^{24}Mg$ of the bracketing DSM standards, namely:

$$\delta^{25}Mg = (^{25}Mg/^{24}Mg)_{Sample}/(^{25}Mg/^{24}Mg)_{DSM\text{-}3} - 1 \qquad \text{Eq. 1}$$

We adhere to IUPAC guidelines (COPLEN 2011) and do not implicitly use a multiplier in the delta terminology but explicitly report any multiplication (e.g. ‰) when presenting data.

We follow the recommendation of YOUNG and GALY (2004) in reporting our mass independent isotope data in logarithmic form, namely as $\Delta'^{26}Mg$ where:

$$\Delta'^{26}Mg = \delta'^{26}Mg - \delta'^{25}Mg/0.511 \qquad \text{Eq. 2}$$

$\delta'^{26}Mg$ and $\delta'^{25}Mg$ are the linearised versions of $\delta^{26}Mg$ and $\delta^{25}Mg$ (see YOUNG AND GALY, 2004), namely;

$$\delta'^{25}Mg = \ln(^{25}Mg/^{24}Mg_{Sample}/^{25}Mg/^{24}Mg_{DSM\text{-}3}) \text{ or } \ln(\delta^{25}Mg+1) \qquad \text{Eq. 3}$$

The numerical values of δ and δ' are very similar but the latter leads to a convenient linear relationship between $\delta'^{26}Mg$ and $\delta'^{25}Mg$ for a given style of fractionation and so a simple expression of mass independent data (Eq 3). The value of 0.511 in Eq. 3 reflects our use of a kinetic fractionation law (see YOUNG AND GALY, 2004). The differences between $\Delta'^{26}Mg$ and conventional $\Delta^{26}Mg$ for the samples reported here are insignificant (in the third decimal place of the values in ppm).

As a main secondary isotopic reference, we used JP-1 which has a matrix composition similar to chondrules. We measured $\Delta'^{26}Mg$ on a number of separate dissolutions of JP-1, including two with sufficient repeat analyses to achieve precisions <±5ppm (Table 2). At least one analysis of JP-1 was made in the same way as samples in each analytical session. Different JP-1 dissolutions were associated with batches 1 (JP-1_1) and batches 2 and 3 respectively (JP-1stock). The latter represents a large stock solution, prepared by combining Mg separated from multiple dissolutions of JP-1. We further measured several other aliquots of JP-1 (Table 2), both processed with hotplate digestions (JP-1m), as above, and using a high-pressure asher (JP-1c), in order to check refractory oxide phases were fully dissolved. A smaller (mg) sample of powder was also analysed to replicate the procedure for a single chondrule (JP-1j). In addition, we measured the basaltic standards BHVO-2 and BIR (Table 2) to provide a reference for matrices with higher aluminium concentrations closer to high Al-chondrules.

The data presented in this study were collected over several years during a period with several different analysts and an evolving measurement protocol. We split our analyses into three periods during which measurement conditions were sufficiently different to merit separate consideration. Our initial approach (during measurement of batch 1 samples) was similar to that previously used for mass dependent measurements (POGGE VON STRANDMANN et al., 2011), but using longer sample analyses to generate more precise $\Delta'^{26}Mg$. Despite greater potential instability of mass bias over these extended sample bracketing timescales, two different dissolutions of JP-1 (JP1_1 and JP-1c) yielded a weighted mean $\delta^{25}Mg$ of -0.13±0.01‰ (Table 2) in good agreement with the value of -0.12±0.04‰ obtained by (POGGE VON STRANDMANN et al., 2011). Subsequent measurements (*i.e.* for batches 2 and 3) were made with rather different focussing conditions, which gave better beam intensity and minimised its decrease over measurement sessions lasting several days. During this period we switched to a configuration using jet and H-cones, rather than normal sample and X-skimmer cones. Although these changes helped in obtaining precise and reproducible mass independent data (see below), the uncertainty on associated

δ^{25}Mg measurements was greater than our previous work (±0.11‰ 2sd, n=206 for JP-1stock). The data using X-cones (±0.12‰ 2sd, n=76) was markedly more variable than for H-cones (±0.08‰ 2sd, n=130) and so for these analytical sessions we only use δ^{25}Mg data measured with H-cones.

The long term average of δ^{25}Mg = -0.18‰ of JP-1stock, obtained using H-cone measurements, was notably low compared to JP-1_1 and JP-1 (chon) and our previous work at Bristol (POGGE VON STRANDMANN et al., 2011). Part of this difference is likely attributable to incomplete sampling of the Mg elution peak during the final stage of chromatographic separation, as discussed above. In the case of JP-1stock, ~3% Mg was lost to the Ni fraction and its δ^{25}Mg is some 0.05‰ lighter than our previous datum. Only two samples were similarly affected by significant Mg loss to the Ni fraction, namely MOK13B (1.8% Mg loss) and 1406-20 (3.9% Mg loss). The magnitude of any effect on δ^{25}Mg should thus be of the order of 0.05‰, by comparison with our stock JP-1, and this has no influence on any of our conclusions.

The values of Δ'^{26}Mg obtained for JP-1 are identical regardless of the minor changes in analytical protocol; 2.1±1.6ppm and 2.0±1.2ppm using X- and H-cones respectively for JP-1stock using the later focus settings and 0.2±3.4ppm for JP1_1 using the original running conditions. So Δ'^{26}Mg measurements from all runs are averaged in calculating the Δ'^{26}Mg of samples reported in Table 2. The consistency of Δ'^{26}Mg for all different JP-1 dissolutions also indicates that minor loss of Mg during the column procedure for JP-1stock (see above) had no significant influence on the mass independent isotope ratio measurement. Our average Δ'^{26}Mg for JP-1 is 1.9±1.0ppm (2se on 258 measurements of 5 different dissolutions over the complete period of analysis). This slightly non zero value indicates that the kinetic law is not a perfect representation of the fractionation processes involved in generating the isotopically heavy composition of DSM-3, and is within error of high precision literature data for another terrestrial peridotite, DTS2 (BIZZARRO et al., 2011; OLSEN et al., 2016). Our values of Δ'^{26}Mg for the basaltic standards BHVO-2 and BIR (Table 2) are also within error of those reported in the literature (BIZZARRO et al 2005, SCHILLER et al. 2010, BAKER et al 2005), but since our measurements of these standards were made with N and X cones in the second period of analysis, we do not report their δ^{25}Mg.

We report measured 2se for the δ^{25}Mg analyses of individual samples in Table 1, but the standard deviation reported for the JP-1 stock (±0.08‰) provides a more realistic estimate of reproducibility for sample-standard

bracketing measurements. We use the latter value in the figures. We have further compared the data obtained by sample-standard bracketing to a method of critical mixture double spiking we have developed (COATH et al. 2017). Agreement is always within the ±0.08‰ 2se error bound placed by repeat JP-1 measurements and is typically much better (Table 2). Since these double spiked measurements were made on solutions already passed through chemistry, they do not provide information on the possible effects of Mg loss during chemistry discussed above.

For our mass independent analyses, precision is dominantly controlled by counting statistics, which is here mainly governed by analysis time. We ran a different number of repeats for different samples and precision is therefore variable but typically we have made sufficient analyses such that Δ'^{26}Mg is <5ppm (2se), see Table 2. In order to provide estimates of uncertainty on Δ'^{26}Mg representative of the whole sample population and analysis period, we report homoscedastic errors. These are calculated using the averaged deviations of all sample and rock standard repeats (see REGELOUS et al., 2008). Given the three distinct periods of analysis, we treated data from each period as representing a single population and calculated the homoscedastic variability for each. For samples measured over different periods of analysis, we calculated uncertainty for averages in each period and took weighted means of these. That measured Δ'^{26}Mg of our different JP-1 dissolutions all lie within their homoscedastic errors (Table 2) indicate this is also an effective measure of sample reproducibility.

3 Results

3.1 Al/Mg variability in chondrules

Major element analyses of the chondrules are reported in Table 1. In order to obtain chronological information, we require chondrules with $^{27}Al/^{24}Mg$ ratios that deviate from a solar value (~0.1), as defined by bulk CI chondrite. Figure 1 shows that $^{27}Al/^{24}Mg$ ratios in our chondrules vary from significantly sub-chondritic (~0.01) to notably super-chondritic (~0.4). These extremes are represented by an isolated olivine (YJ7) and high-Al chondrule (YJ10) respectively, but the more typical ferromagnesian chondrules also show marked variability in $^{27}Al/^{24}Mg$ (0.036-0.275). Our first batch of eight chondrules only contained three with non-chondritic $^{27}Al/^{24}Mg$, including the Al-rich chondrule. For our second and third batches of samples, we used pixel counting to estimate the proportion of each mineral phase present in elemental X-ray maps and calculated approximate $^{27}Al/^{24}Mg$ ratios using the mineral compositions. We screened fifty chondrules (33 from Mokoia and 17 from

Vigarano) and identified 18 chondrules with estimated $^{27}Al/^{24}Mg \leq 0.05$ or $^{27}Al/^{24}Mg \geq 0.20$, of which we analysed 13. The $^{27}Al/^{24}Mg$ ratios estimated from the X-ray maps are not well correlated with those subsequently determined by quadrupole ICP-MS, presumably from a combination of intrinsic inaccuracy of the compositional reconstruction and that the sections examined were not necessarily representative of the entire chondrule (e.g. FRIEND et al., 2016). Nonetheless, the screened batches of chondrules did yield a larger proportion with non-chondritic $^{27}Al/^{24}Mg$ ratios compared to populations reported in the literature (JONES AND SCHILK, 2009) and the unscreened batch (Fig. 1a).

The relative abundances of other major elements provide additional information on the origin of variability of $^{27}Al/^{24}Mg$ ratios. Since these data were measured on aliquots of the same solutions analysed for Mg isotopes, they are a direct monitor of associated compositional changes. The variability of Al in the chondrules correlates well with other 'incompatible' elements that are excluded from the ferromagnesian phases during crystallisation of chondrules (Fig. 1b &c). This observation pertains to elements that are both refractory (Ti) and volatile (Na).

3.2 Petrography of the chondrules

Most of the chondrules we analysed were porphyritic olivine pyroxene (POP) type, but there were also two porphyritic olivine (PO), one porphyritic pyroxene (PP), one barred olivine (BO) and one Al-rich chondrule (Table 1). The proportion of petrographic types in screened and unscreened batches are similar. False colour X-ray images of each chondrule can be found in Appendix 1, but brief summaries of the mineralogy and main textural features are provided below.

The great majority of chondrules studied are Type I, Fe-poor chondrules. Electron microprobe compositions of analysed minerals are reported in Appendix 2 and summarised for olivine and low-Ca pyroxenes in Fig. 2. Only three chondrules (YJ7, YJ5 and YJ10) have average olivines compositions with Mg# <90 (where Mg#=100xMg/(Mg+Fe) for molar abundances of Mg and Fe). One of these, YJ7, is an isolated olivine of >300μm diameter, which zones from a Mg#80 core to ~ Mg#60 rim and is presumably derived from a Type II chondrule (e.g. JONES, 1992). In contrast, we suggest the low Mg# olivines in YJ5 (a POP chondrule from Allende) and YJ10 (the high-Al chondrule from Mokoia, see below and Fig. 3a) reflect ingress of iron during parent body metamorphism. Several of the other chondrules show less extreme signs of alteration on portions of the imaged samples (e.g. YJ6, YJ4, MOK4 and 1406-20), see Fig. 3b. Most chondrules have interstitial

plagioclase and Ca-rich overgrowths of low Ca-pyroxene (Appendix 1), but chondrules MOK3 and YJ9 are mesostasis-rich and contain no interstitial plagioclase.

The dominant POP chondrules show a range of textures, from those dominated by fine grained olivines with occasional larger pyroxene grains (Fig. 3c, VIG 1), to larger olivines in the core and coarse rims of euhedral pyroxene in reaction texture with the olivines (Fig. 3d, 1406-1), to more extensive reaction of olivine to pyroxene throughout the chondrule (Fig. 3e, VIG6A). Although some of the differences between textures exemplified by Fig. 3d and Fig. 3e may reflect the line of section taken and its proximity to a chondrule rim (e.g. FRIEND et al., 2016)), the textural contrast between Fig. 3c and Fig. 3d appears distinct.

YJ10 is an unusual Al-rich chondrule that has been fractured into several pieces ~100 – 400 μm in size during the polishing process. The fragments we have available for petrographic study (Fig. 3a) are unrimmed, and dominated by angular Ti-bearing (>2 wt. %) diopside (Wo_{55}) enclosing minor olivine (Fo_{73}). Rare spinel grains are subhedral and embedded within diopside and anorthite. Olivine has Fe-rich rims. Evidence of low temperature metasomatism is present: anorthite has been partially replaced by sodalite ($Na_8[Al_6Si_6O_{24}]Cl_2$) and hedenbergite grains ($FeCaSi_2O_6$) are also present.

MOK13B is petrographically unique, being dominantly a highly forsteritic olivine with high Ca and Ti contents (Table 1, Appendix 2), with spinel inclusions and patch of intergrown laths of anorthite and diospide (Fig. 3f). The composition of the olivine is the same as that of refractory forsterite reported in several chondrites and the texture is reminiscent, for example, of a refractory forsterite-bearing chondrule RF16 reported in Fig. 1a from PACK et al. (2004).

3.3 Mg isotopic compositions of the chondrules

Our chondrules show a range in mass-dependent Mg isotopic compositions (Fig. 4a), with δ^{25}Mg varying from -0.27 to +0.24‰, relative to a bulk chondritic reference of -0.15±0.04‰ (TENG et al., 2010). In keeping with several recent bulk chondrule studies (BOUVIER et al 2013; OLSEN et al., 2016; VAN KOOTEN et al., 2015), the δ^{25}Mg of our individual chondrules scatter to either side of bulk chondrite, but there is a preponderance of slightly isotopically heavy compositions (-0.1 to 0‰) and occasional, substantially higher values (Fig. 4a). Unlike some previous studies (BIZZARRO et al., 2004; GALY et al., 2000; OLSEN et al., 2013), we do not see a

correlation between $\delta^{25}Mg$ with $^{27}Al/^{24}Mg$ (Fig. 4b), although our chondrules do not range to such high $^{27}Al/^{24}Mg$ as the former two studies (BIZZARRO et al., 2004; GALY et al., 2000).

Figure 5 shows an 'isochron' plot of $^{27}Al/^{24}Mg$ vs $\Delta'^{26}Mg$. The chondrules as a whole form a broadly positive array, with upper bound marked by two ferromagesian and the Al-rich chondrule. Seven chondrules have $\Delta'^{26}Mg$ clearly distinct from an unfractionated, 'chondrule reservoir' composition (horizontal grey bar in Fig. 5), inferred from a weighted mean of chondrules with solar $^{27}Al/^{24}Mg$ (see section 4.2). The Al-rich chondrule from Mokoia and five ferromagesian chondrules have elevated $\Delta'^{26}Mg$ whilst the relict olivine MOK13B has markedly negative $\Delta'^{26}Mg$. Despite a range in their $^{27}Al/^{24}Mg$, the other chondrules fall within error of the chondrule reservoir value.

4 Discussion

4.1 Extent of thermal metamorphism

CV chondrites, while exhibiting primitive textures, show evidence for having experienced parent body thermal metamorphism. Secondary processing can disturb the Al-Mg system and result in isochrons that do not accurately reflect the timing of the last reset event (e.g. MARUYAMA AND YURIMOTO, 2003). BONAL et al. (2006) showed that the petrographic subtype for Allende is >3.6; for Mokoia CV3.6 and for Vigarano CV3.1-3.4. KROT et al. (1995) showed that Allende has experienced a complex parent body history including hydration of matrix silicates and dehydration to form fayalite. Work by JONES AND SCHILK (2009) recorded that the majority of chondrules in Mokoia have experienced minimal metamorphism (petrologic type < 3.2), but Mokoia is a complex breccia with clasts of heavily aqueously altered material (TOMEOKA AND OHNISHI, 2014). Our Mokoia chondrules are clearly a mixture of those that have been extensively altered by parent body processes (e.g. JY10) and those that have been relatively unscathed (e.g. MOK5, MOK 13B).

The extent of chondrule metamorphism has been linked with the FeO and CaO contents of their olivine, due to diffusive exchange between phases in chondrules and the surrounding matrix. Most of our ferromagnesian chondrules have olivine Mg# (Fig. 2) and CaO contents (Appendix 2) that fall in the Type 3.3-3.4 field of SCOTT et al. (1994), indicating comparable, modest degrees of parent body metamorphism. This limited Fe-Mg equilibration with the surrounding matrix suggests that the Mg isotope composition of the bulk chondrule is

likely only lightly modified after emplacement in the meteorite parent body. Occasional analyses of lower Mg# (Fig. 2) show localised alteration by fluids, as noted petrographically (section 3.2). The Al-Mg systematics of the latter chondrules should thus be interpreted with some caution.

355

4.2 *Bulk chondrule model ages*

The slope defined by closed system, cogenetic samples on an isochron diagram such as Fig. 5 has chronological significance. If chondrules were formed from a homogenous nebula, the slope of a line joining solar and chondrule compositions yields the $(^{26}Al/^{27}Al)_0$ at the time of Al/Mg fractionation from solar to chondrule value:

360 $$\text{slope} = (^{26}Al/^{27}Al)_0^{\text{prescursor}} = [(^{26}Mg/^{24}Mg)^{\text{sample}}-(^{26}Mg/^{24}Mg)^{\text{solar}}]/[(^{27}Al/^{24}Mg)^{\text{sample}}-(^{27}Al/^{24}Mg)^{\text{solar}}] \quad \text{Eq. 4}$$

Given a known, uniform nebula $(^{26}Al/^{27}Al)_0$, this then gives the time of this fractionation:

$$t_{frac} = \ln [\text{Isochron slope}/ (^{26}Al/^{27}Al)_0^{\text{solar}}]/-\lambda^{26Al} \quad \text{Eq. 5}$$

As stressed previously, such bulk chondrule "ages" give the time of their precursor formation, rather than the chondrule melting event itself.

365 An initial concern, however, is establishing a suitable reference point (the 'pivot' point in Fig. 5) for calculating model ages. As discussed in the idealised scenario above, the pivot point represents an unfractionated solar composition, but more specifically for this study it should constitute a hypothetical bulk CV chondrule reservoir. CI chondrites are frequently used to represent unfractionated, solar compositions, but recent work has demonstrated that mass independent isotopic compositions of different chondrite groups are variable (LARSEN et 370 al 2011, VAN KOOTEN et al 2015, OLSEN et al 2016, LARSEN et al 2016). Thus, CI chondrites may not provide a valid bulk Mg isotopic composition for CV chondrules. Yet, finding robust alternative is challenging. A bulk CV analysis might seem an attractive choice, but this poses significant practical difficulties in sampling a truly representative average (see STRACKE et al, 2012) especially given the substantial influence of CAI on the Mg isotope systematics (see section 4.6). Moreover, whether or not the contribution of CAI should be included in 375 the bulk chondrule reference is moot. Obtaining a representative sample of the matrix is an experimentally more tractable proposition but given the apparently complementary nature of chondrules and matrix (e.g. PALME et al 2015) it may not be appropriate.

In addressing this problem, we infer that the bulk chondrule reservoir should be represented by a solar composition in terms of its major element abundances, but that we need to independently define its Mg isotopic composition. This approach is similar to that used by OLSEN et al (2016). To this end, we averaged the Δ'^{26}Mg of our three chondrules that have $^{27}Al/^{24}Mg$ within error of the 'solar', CI value (~0.1, e.g. WASSON AND KALLEMEYN, 1998). Interestingly, the weighted average we derive ($\Delta'^{26}Mg = 2.9\pm2.1$ppm) is indistinguishable from average CI (4.2±1.3ppm), as determined by LARSEN et al, 2011. Furthermore, using this unfractionated CV chondrule reservoir reference (hereafter 'chondrule reservoir') none of our data fall in the "forbidden zone" of the isochron diagram, i.e. in the top left or bottom right fields defined by CAI array and horizontal line with 'chondrule reservoir' Δ'^{26}Mg, see Fig. 5. These observations provide empirical support for our choice of 'chondrule reservoir' Δ'^{26}Mg. We acknowledge that the notion of a bulk chondrule reservoir is simplistic given the petrological and geochemical complexity evident in chondrules, but this allows us to make first order chronological inferences. Applying Occam's razor, we first explore these most straight-forward interpretations before considering alternative scenarios.

In Fig. 5 we show three reference lines. The steepest line is defined by CAI that have undergone closed system evolution with $(^{26}Al/^{27}Al)_0 = 5.23x10^{-5}$ (JACOBSEN et al., 2008). The two shallower slopes have $(^{26}Al/^{27}Al)_0$ of $2x10^{-5}$ and $0.76x10^{-5}$ and so are two-stage model isochrons of Al-Mg fractionation from a solar value at 1 and 2Ma post CAI, assuming canonical, homogenous solar system $(^{26}Al/^{27}Al)_0$. Our most radiogenic chondrules lie within these bounds (Fig. 5), suggesting their precursors formed over this ~1Ma period. For many of our chondrule analyses, however, relatively small deviations in their $^{27}Al/^{24}Mg$ from solar makes it impossible resolve the possible original presence of finite ^{26}Al given the precision of our Δ'^{24}Mg measurements. Whilst a number of chondrules lie on the line defining $(^{26}Al/^{27}Al)_0 = 0.76x10^{-5}$, many of these equally have Δ'^{24}Mg within error of the 'chondrule reservoir' and so potentially $(^{26}Al/^{27}Al)_0 = 0$. We have calculated model $(^{26}Al/^{27}Al)_0$ of individual chondrules, from two point isochrons with the 'chondrule reservoir'. These values are reported in Table 3 (also expressed as model ages, using different solar system $(^{26}Al/^{27}Al)_0$). All model $(^{26}Al/^{27}Al)_0$ outside error of zero are plotted in Fig 6.

There are two samples, a Vigarano chondrule (1406-20) and an isolated olivine from Allende (YJ7), that have sufficiently low $^{27}Al/^{24}Mg$ that their absence of associated Δ'^{26}Mg deficits is significant. At face value the precursors of these samples need to have formed after the decay of ^{26}Al (which subsequently we nominally take to be >2Ma post CAI, given our effective temporal resolution), once Δ'^{26}Mg of the nebula ceased to evolve.

One of these samples (1406-20) shows clear evidence for parent body alteration in terms of variable olivine Mg# (Fig. 2) and petrographic observations (Fig. 3b) and so its $\Delta'^{26}Mg$ may reflect metamorphic resetting. Nonetheless, the most obviously altered chondrule, the Al-rich chondrule YJ10 (Fig. 3a) retains a radiogenic signature and so parent body alteration does not necessarily reset Al-Mg systematics in these low-grade meteorites. Concerns over alteration do not pertain to the other sample with low $^{27}Al/^{24}Mg$ (YJ7) that yields a young model age (>2Ma post CAI). In contrast, the very negative $\Delta'^{26}Mg$ of the Mokoia relict grain (MOK13B), Fig. 5, points to early formation, in keeping with its refractory nature (section 3.2). The model age for MOK13B gives a time of precursor formation 0.47Ma post CAI. This is ~0.5Ma older than the oldest model precursor ages we inferred above for more typical ferromagnesian chondrules (Table 3).

We have assumed a canonical solar system $(^{26}Al/^{27}Al)_0$ that was constant across CAI and chondrule forming reservoirs in the model ages discussed above. Recent work has argued for heterogeneous $(^{26}Al/^{27}Al)_0$ in the solar proto-planetary disk, with a higher initial value in CAIs than bulk chondrites (LARSEN et al., 2011; SCHILLER et al., 2015). In this case, the chondrule ages we infer would be older. For example, OLSEN et al 2016 propose $(^{26}Al/^{27}Al)_0 = 2.2x10^{-5}$ for the CV chondrule reservoir. This is based on the average $\Delta'^{26}Mg$ of their chondrules with solar $^{27}Al/^{24}Mg$, assuming a closed system evolution from an initial, homogeneous initial solar system $\Delta'^{26}Mg$ = -15ppm, derived from the Larsen et al 2011 CAI-AOA (ameboidal olivine aggregate) isochron. Using their inferred CV chondrule reservoir $(^{26}Al/^{27}Al)_0$, four of our chondrules yield precursor model ages as old as CAI (Table 3). In this scenario suggested by OLSEN et al 2016, however, no object can have an initial $\Delta'^{26}Mg$ less than 15ppm. This is contravened by our refractory object MOK13B, which has measured $\Delta'^{26}Mg$ = -16.5±2.9ppm. When conservatively corrected for *in situ* decay, using measured $^{27}Al/^{24}Mg$ and $(^{26}Al/^{27}Al)_0 = 2.2x10^{-5}$, MOK13B yields an initial $\Delta'^{26}Mg$ = -21±2.9ppm.

More complex models can be envisioned, but the unradiogenic nature of MOK13B, if representative of the CV chondrule reservoir, places useful constraints on its minimum $(^{26}Al/^{27}Al)_0$. Assuming MOK13B was derived from a chondrule reservoir with present day $\Delta'^{26}Mg$ = 2.9ppm (as described above), the reservoir had $(^{26}Al/^{27}Al)_0 > 3.4±0.8x10^{-5}$. We calculate a further set of model precursor ages for our chondrules using this minimum value (Table 3).

Alternatively, WASSERBURG et al. (2012) pointed to Mg isotope heterogeneity in different CAIs, suggesting that wider-spread heterogeneity amongst chondrite bodies which might account for the features reported by LARSEN

et al. (2011). Given we derive age constraints from different chondrules found within the same parent body, gross differences in the Mg isotope compositions between chondritic bodies will not influence our calculated relative age differences. Admittedly, mass independent Ti (TRINQUIER et al., 2009) and Cr isotopic heterogeneities (OLSEN et al., 2016) have been reported between individual chondrules from CV chondrites, showing they are not co-genetic. We have not made such analyses on our samples. If there were significant initial $^{26}Mg/^{24}Mg$ heterogeneity between chondrules this could account for some $\Delta'^{26}Mg$ variability. Yet, in the data of OLSEN et al, 2016 there is no systematic relationship between the minor differences in $\Delta'^{26}Mg$ and a wide range in $\varepsilon^{54}Cr$ of individual chondrules, suggesting this is not a major consideration.

4.3 *Origin of variable Al-Mg in chondrules*

In order to understand what process is being dated by the Al-Mg systematics, we need to explore the causes of the variable $^{27}Al/^{24}Mg$ of the chondrules. An obvious initial question is whether Al-Mg fractionation occurred during chondrule formation or was inherited. So far, we have generally noted that the model ages date the fractionation of Al-Mg in the chondrule precursors, but it is possible that this fractionation occurred during flash melting of the chondrule,

Preferential Mg evaporation relative to refractory Al (and Ti) is a possible means to explain a range of $^{27}Al/^{24}Mg$ to elevated values by a process intrinsically related to chondrule formation (GALY et al., 2000; OLSEN et al., 2013). If partial evaporation occurs under conditions of high gas pressure, sufficient Mg loss is possible without excessive Mg isotopic fractionation (GALY et al., 2000) or loss of other volatile elements (ALEXANDER et al., 2008). However, several lines of evidence argue against a dominant role for partial evaporation as a means of increasing the $^{27}Al/^{24}Mg$ in the chondrules of this study. Firstly we observe no systematic change in $\delta^{25}Mg$ with increasing $^{27}Al/^{24}Mg$ (Fig. 4a). Although high gas pressures can suppress fractionation it will not be eliminated entirely, and indeed CB chondrules reported by OLSEN et al. (2013) do show increasing $\delta^{25}Mg$ with $^{27}Al/^{24}Mg$ (Fig. 4b). Secondly, high gas pressure may limit loss of volatile elements, but for our chondrules sodium contents increase with those of refractory elements (Fig. 1c), which is not anticipated as a result of evaporation alone. Thirdly, partial evaporation can account for chondrules with super-chondritic $^{27}Al/^{24}Mg$, but cannot readily explain the chondrules with sub-chondritic $^{27}Al/^{24}Mg$ (<0.1).

Finally, many of the Al-rich chondrules argued to be the product of partial evaporation by GALY et al. (2000) have compositions that can also be well explained by mixing with CAI (Fig. 4b), see section 4.6.

We argue that a more likely origin for the range in $^{27}Al/^{24}Mg$ of our ferromagnesian chondrules is reworking of fragments from previous generations of chondrules (see JONES AND SCHILK, 2009). Olivine (or pyroxene) and mesostasis (or fine-grained phases crystallised from it) that grew during cooling of earlier-formed chondrules have low and high $^{27}Al/^{24}Mg$, (Ti/Mg and Na/Mg) respectively. Remixing these components in variable proportions can account for the variability in major element compositions observed in our samples (Fig. 1). Pristine model ages potentially reflect several episodes of mixing and fractionation rather than a simple, single events.

4.4 *Variable model ages and chondrule-vapour interaction*

The Al-Mg systematics of reworked chondrule fragments will depend not only on the timing of prior fractionation but also any subsequent chemical exchange. The range in model $(^{26}Al/^{27}Al)_0$ evident in Fig. 6, may reflect a protracted period of chondrule formation (as precursors for subsequent chondrules) in the protoplanetary disk. Alternatively, the range in model ages could represent chondrules formed from precursors of similar age, reworked and reset at variable times (see evidence for multiple chondrule heating reviewed in JONES et al., 2005). More complex variants are also possible, for example, there may have been different extents of partial resetting. The latter scenarios require chemical interaction between the chondrules and their surroundings during reworking. This could plausibly occur during a high energy event, similar to the original chondrule forming episode, in an environment which generated a silicate vapour atmosphere. Several studies have invoked vapour-chondrule interaction to account for important features of chondrules such as the commonly observed mantles of pyroxene surrounding a more olivine-rich core (LIBOUREL et al., 2006; MARROCHI AND CHAUSSIDON, 2015; TISSANDER et al., 2002). This process may also affect Mg abundances (NAGAHARA et al., 2009) and alter the mass dependent Mg isotope composition of the resulting chondrules (USHIKUBO et al. 2013). Here we further consider that Mg isotopic exchange between pre-existing chondrules and the chondritic silicate vapour could modify its $\Delta'^{26}Mg$.

To see how these processes might pertain to our samples, we focus on chondrules with super-chondritic $^{27}Al/^{24}Mg$ but a range of $\Delta'^{26}Mg$. For example, VIG1 and 1406-1 both have $^{27}Al/^{24}Mg$ ~0.2 but variable

Δ'^{26}Mg which results in model precursor $(^{26}Al/^{27}Al)_0$ of $2.1x10^{-5}$ and $0.7x10^{-5}$ respectively. The petrography of these chondrules is shown in Figs. 3c and d. A key difference is that the less radiogenic 1406-1 has a notable low-Ca pyroxene mantle. Reheating of a chondrule such as VIG 1 in a solar, SiO-rich vapour will lead to the growth of a pyroxene mantle (e.g. LIBOUREL et al., 2006) and exchange with the less radiogenic (chondritic) Mg of the gas. In general, chondrules in our study with the most radiogenic Δ'^{26}Mg appear to have the least developed low-Ca pyroxene rims. Equally sample VIG6a, which has sub-chondritic $^{27}Al/^{24}Mg$ sample but lacks a Δ'^{26}Mg deficit, has extensively developed poikilitic low-Ca pyroxene (Fig. 3e). This again points to its later interaction with a silicate vapour. If the vapour had a chondritic composition and interaction occurred after ^{26}Al had decayed, then Δ'^{26}Mg is reset to the 'chondrite reservoir' value observed. These arguments have resonance with those of TACHIBANA et al. (2003), who noted a correlation of the ages of chondrules and their SiO_2 content (although such a correlation was not confirmed in a later, more precise study by VILLENEUVE ET AL., 2012).

4.5 *CAI component in high Δ^{26}Mg chondrules?*

Some of the variations in Δ'^{26}Mg observed in Fig. 5 could potentially reflect mixing between an old, radiogenic refractory component (e.g. CAI) and bulk chondritic material. This notion was explored and rejected by Bizzarro et al (2004) on the basis of the systematics of mixing between bulk chondritic material and CAI on a plot of δ^{25}Mg vs Δ^{26}Mg. Since then a wider range of bulk CAI compositions have been reported that negate these original arguments (see Fig. 7a). In Figure 7a, samples that lie above the dashed lines may be explained by mixing between a chondritic composition and known CAI or AOA (Fig. 7b). Mixing with the commonest CAI compositions (see Fig 7b) will form an oblique mixing line in Figure 7a. Some of the samples from BIZZARRO et al. (2004) and GALY et al. (2000) plausibly fall on such mixing lines (those indicated with white dashes in Fig. 7a). Given a strong petrographic link between some high Al chondrules and refractory inclusions (see RUSSELL et al., 2005) and their oxygen isotope relationships (MCKEEGAN et al., 1998), the potential role of CAI in accounting for the Mg isotope systematics of high-Al chondrules is unsurprising. The involvement of CAI for a number of bulk chondrules from BIZZARRO et al (2004), which have $(^{26}Al/^{27}Al)_0$, within error of CAI, would help explain these unusually high values coupled with elevated δ^{25}Mg (Fig. 8).

In our study, however, the ferromagnesian chondrules with significantly super-chondritic Δ'^{26}Mg have indistinguishable δ^{25}Mg from bulk chondrites. This is inconsistent with the great majority of CAI–chondrite

mixing scenarios (Fig. 7b). Yet CAIs and AOAs have a wide range of compositions, albeit some measurements may be potentially contaminated with matrix (GOUNELLE et al., 2007). Their variability makes it difficult to rule out the possibility of a CAI component in our chondrules, especially for the high Al/Mg chondrule JY10. Yet the major element systematics of our chondrules are inconsistent with CAI mixing (Fig 1c). The scarcity of diagnostic, CAI-REE patterns in Mokoia chondrules (JONES AND SCHILK, 2009) further argues against a CAI component being responsible for most ferro-magnesian chondrules with relatively high $^{27}Al/^{24}Mg$. Importantly, mixing with a high A/Mg CAI cannot generate the unradiogenic relict olivine composition with the oldest model age.

For the chondrule analyses of this study, it is notable that of the samples with super chondritic $^{27}Al/^{24}Mg$, those which have elevated $\Delta'^{26}Mg$ and old model precursor ages have chondritic $\delta^{25}Mg$, whereas those with lower, potentially reset $\Delta'^{26}Mg$, have anomalously high $\delta^{25}Mg$ (Fig. 7a). These systematics are incompatible with involvement of CAI material but are consistent with silicate rich gas interaction lowering $\Delta'^{26}Mg$ and elevating $\delta^{25}Mg$ in the chondrule (Fig 7b).

4.6 *Comparison of our data with other chondrule chronologies*

In this section we compare our model ages with data from *in situ* Al-Mg mineral isochrons (e.g. KITA and USHIKUBO, 2012) and Pb-Pb isochrons from multiple leach steps (e.g. CONNELLY et al. 2012). These isochron approaches date the crystallisation of chondrules, rather than the fractionation of its composition from an evolving chondritic/nebula reference, as determined by bulk analyses. These different approaches therefore need not record similar ages.

For the Al-Mg system we can compare the $(^{26}Al/^{27}Al)_0$ of internal isochron and bulk measurements rather than turn this ratio into a model age. Figure 6 contrasts the $(^{26}Al/^{27}Al)_0$ of our bulk analyses with more some recent, high precision studies that report numerous internal chondrule isochrons on single primitive meteorites (KURAHASHI et al., 2008; LUU et al., 2015; VILLENEUVE et al., 2009). We also show the two oldest reported ages for primitive chondrites (MOSTEFAOUI et al., 2002; RUSSELL et al., 1997). The range of model $(^{26}Al/^{27}Al)_0$ we document for bulk CV chondrules agrees well with the *in situ* values for Allende chondrules reported by Luu et al. (LUU et al., 2015). The latter work also obtained consistent *in situ* measurements and bulk model ages on

545 the same chondrules, but these direct comparisons were limited to Al-rich chondrules. The maximum $(^{26}Al/^{27}Al)_0$ found in ion-microprobe studies of ordinary chondrites (MOSTEFAOUI et al., 2002; RUSSELL et al., 1997) are also in line with the highest values from our bulk analyses. Comparison of the frequency of younger ages by the different analytical approaches is difficult, given bulk measurements of ferromagnesian chondrules are less effective at resolving these lower values (see section 4.2). For many of our chondrules, for example, we
550 cannot distinguish between $(^{26}Al/^{27}Al)_0 \sim 7.6x10^{-6}$ and no extant ^{26}Al (see Fig. 5).

Given the different processes recorded by the $(^{26}Al/^{27}Al)_0$ of bulk analyses and internal isochrons, it is striking that a maximum value of $(^{26}Al/^{27}Al)_0$ in typical ferro-magnesian chondrules is similar for both techniques and likewise both approaches show a range in $(^{26}Al/^{27}Al)_0$. An explanation for these observations would be a protracted period of chondrule formation, in which older generations of chondrules are rapidly reworked giving
555 some coherence of maximun crystallisation and precursor ages. Bulk chondrules analyses are likely to be more robust to resetting during high temperature thermal reprocessing than internal isochrons which are frequently pinned by analyses of mesostasis and this may explain the preliminary observation that there are a greater proportion of higher $(^{26}Al/^{27}Al)_0$ values by this technique. Nonetheless reheating must be sufficiently intense that bulk and *in situ* ages are often fully reset, by complete remelting and re-equilibration with a chondrule
560 reservoir vapour.

Our oldest model ages document the fractionation of Al-Mg in ferromagnesian materials within 0.5Ma of CAI (Table 3), within error of the oldest Pb-Pb chondrule ages. At face value, our range in model precursor ages also seem pleasingly compatible with the spread Pb-Pb ages of individual chondrules and the extended period of reworking inferred from these observations (CONNELLY et al., 2012, BOLLARD et al. 2017). In detail, we require
565 that reworking of chondrules involves not just remelting but interaction with a vapour atmosphere, to cause resetting of Mg isotope compositions to a chondrule reservoir value. For this to be consistent with the Pb-Pb measurements, Pb exchange with the vapour must either be limited or the vapour have a radiogenic composition, i.e. derived from vapourising chondrules rather than a solar composition. It is not implausible to envisage such scenarios, but further discussion is perhaps not warranted until high precision Pb-Pb and Al-Mg
570 data on the same chondrules are published in the literature.

Comparison of our data with a mean Hf-W age of 2.2±0.8Ma post CAI, derived from analysis of hundreds of Allende chondrules (BUDDE et al., 2016) is complicated by the difficulty in determining a mean model age for our sample set with many values in error of infinity, in addition to uncertainty in the chondrule reservoir

$(^{26}Al/^{27}Al)_0$. Nonetheless, it is quite possible that our data might yield a consistent mean Al-Mg model fractionation age of ~2Ma post CAI (Table 3).

4.7 *Comparison with other bulk chondrule studies*

There have been several recent studies on chondrules from CV, CR, CH/CB and CB meteorites reporting Mg isotope measurements as precise or better than reported in our work (OLSEN et al., 2013; OLSEN et al., 2016; VAN KOOTEN et al., 2015). After careful consideration of the style of mass fractionation (OLSEN et al., 2013), the CB chondrules show no significant variability in $\Delta'^{26}Mg$ (see Fig 8), as was documented in an earlier, lower precision study (GOUNELLE et al., 2007). OLSEN et al. (2013) argue their observations are in keeping with a young age of chondrule formation in CB chondrites (BOLLARD et al., 2015; KROT et al., 2005) and so this work does not provide clear points of comparison with the $\Delta'^{26}Mg$ of this study. The Al-Mg systematics of chondrules from CR and the CH/CB meteorite Isheyevo are in striking contrast to most bulk CV chondrules, as presented here and in the literature (BIZZARRO et al., 2004; GALY et al., 2000; LUU et al., 2015). These samples show low $\Delta'^{26}Mg$ (~ -16-0ppm) across variable $^{27}Al/^{24}Mg$ (Fig. 8). The authors attribute this observation to an absence of live ^{26}Al in the CR clan meteorites, which they also invoke to help account for their low $\Delta'^{26}Mg$.

The work of OLSEN et al. (2016) on CV chondrules from chondrites Vigarano and NWA 3118 provides a direct comparison with our study. Despite a similar range in $^{27}Al/^{24}Mg$ to our CV chondrules, the samples of OLSEN et al. (2016) show minimal variation in $\Delta'^{26}Mg$ (Fig. 5). This array yields a slope implying precursor $(^{26}Al/^{27}Al)_0$ $\sim 2x10^{-6}$. This value is lower than that obtained for *in situ* analyses of Allende chondrules (LUU et al, 2015), Fig. 6. We therefore infer that the CV chondrules reported by OLSEN et al (2016) must have experienced late Mg isotope exchange with a silicate vapour as we infer for many of our chondrules. It is would appear that OLSEN et al 2016 sampled exclusively such reset chondrules.

5 Summary

Our analyses document a series of events occurring in the early solar system. A refractory olivine carries a record of early igneous mineral growth, that fractionated Mg from Al at <0.5Ma post CAI. The oldest normal, ferro-magnesian chondrules have model ages of precursor formation <1Ma post CAI and a range of younger

model ages until a time when ^{26}Al was extinct (>2Ma post-CAI if $^{26}Al/^{27}Al$ was initially homogeneous), likely reflecting variable resetting of Mg isotopic compositions with a silicate vapour phase. We suggest that Al-Mg fractionation in chondrule precursors is generated in prior chondrule formation and non-quantitative reworking of the products of chondrule crystallisation into subsequent generations of chondrules. Bulk chondrule Al-Mg systematics thus provide evidence of >2Ma of chondrule formation and recycling. Parent body processes may have further affected the bulk Mg isotope systematics, but likely to a minor degree for our key samples.

Acknowledgements

We are grateful to Stanislav Strekopytov, John Spratt & Anton Kearsley, Natural History Museum for technical support, and to Carolyn Taylor and Tu-Han Luu, Bristol for discussions and technical assistance. Meteorites were provided by the Natural History Museum. The paper benefitted from three thoughtful and thorough reviews. This work was funded by STFC grant ST/J001473/1 and ERC grant ISONEB 321209.

Table and Figure Captions:

Table 1 Weights, petrography and relative elemental abundances of bulk chondrules. Elemental data are reported as weight ratios, except $^{27}Al/^{24}Mg$ which are atomic ratios. The samples were processed in three batches, which are indicated. The weights reported are for the chondrule after isolation and cleaning, but before splitting. Abbreviations for petrographic textures given in main text. Also reported are data obtained on two dissolutions of the standard JP-1 run together with batches 2 and 3 (the aliquot of JP-1 processed with sample 1 was not analysed for element abundances). Reference values for JP-1 are taken from Imai et al. (1995) except for Ti, which comes from MAKISHIMA AND NAKAMURA (2000).

Table 2 Al-Mg isotope systematics for bulk chondrules. Means of 'n' repeat analyses are reported. Uncertainly reported as 2 standard errors of the mean for each sample ($\delta^{25}Mg$) or a homoscedastic statistic ($\Delta'^{26}Mg$) calculated from all samples and standards for a given measurement period (see main text). Separate JP-1 analyses documented include: ~1mg (chondrule-sized) aliquot (JP-1j), ~10mg aliquots dissolved by standard (JP-1_1, JP-1m) and high pressure ashing (JP-1c) approaches and a 'stock' solution (JP-1 stock), which represents the homogenised Mg fraction of 8 separate ~10mg dissolutions. Two standard deviations of 130 measurements of JP-1 stock made using jet and H cone configuration are reported as an estimate the reproducibility of the $\delta^{25}Mg$ sample-standard bracketing data. The data labelled $\delta^{25}Mg$ (DS) are critically double-spiked mass-dependent Mg isotope data (COATH et al., 2017) measured on a sub-set of samples to compare with the sample-standard bracketed $\delta^{25}Mg$.

Table 3 Model bulk chondrule precursor $(^{26}Al/^{27}Al)_0$, calculated using equations 4 and 5 and a 'chondrule reservoir' reference (solar) composition. Cited uncertainty includes propagated 2se of sample analysis and 2se in weighted mean of 'chondrule reservoir'. The model $(^{26}Al/^{27}Al)_0$ are also presented as model precursor "ages" using three different values for $(^{26}Al/^{27}Al)_0$ of the 'chondrule reservoir': a canonical CAI value ($5.23x10^{-5}$, JACOBSEN et al, 2008), the proposed value for CV3 by OLSEN et al. (2016), and an empirical (minimum) value from this study ($3.4x10^{-5}$) assuming MOK13B formed contemporaneously with CAI and constitutes a representative sample of the initial 'chondrule reservoir'. The 2se uncertainties in the model "ages" are the same regardless of chosen $(^{26}Al/^{27}Al)_0$ and so only reported once. Model $(^{26}Al/^{27}Al)_0$ are only given for samples that yield positive values. Undetermined upper bounds on model "ages" are marked 'inf'. Associated samples are italicised and not plotted in Fig. 6.

Figure 1 a) Distribution of $^{27}Al/^{24}Mg$ (atomic ratios) in chondrules of this study contrasted with a larger sample set of chondrules from the CV chondrite Mokoia (JONES AND SCHILK, 2009). Histograms are shown for sample batches both screened using SEM images to try to select for samples with non-chondritic $^{27}Al/^{24}Mg$ (see text) and unscreened. $^{27}Al/^{24}Mg$ (atomic ratios) versus b) Ti/Na (weight ratio) and c) Na/Mg (weight ratio) for the samples analysed in this study.

Figure 2 Composition of major mafic phases in chondrules of this study expressed as molar Mg/(Mg+Fe)x100 (Mg#). Analyses of individual points (smaller symbols) and chondrule averages (bold symbols) are shown for olivine (red) and low-Ca pyroxene (blue). One Allende chondrule plotted on right hand side (YJ7) is an isolated olivine containing no pyroxene. Three spot analyses of YJ5 and four of YJ7 that have Mg# between 60 and 70 are not shown so as not to unduly compress the scale.

Figure 3 Representative petrography of chondrules, illustrated using false colour X-rays maps (colours ascribed as shown in key) a) YJ10, an Al-rich chondrule, showing alteration of pale purple anorthite cores to darker purple sodalite b) 1406-20, a porphyritic pyroxene chondrule, with a small core of olivine just visible within low-Ca pyroxene. The feldspathoid alteration product of Na-feldspar can be seen as blue crystal on upper right edge. c) VIG1, a porphyritic olivine-pyroxene chondrule, has abundant, fine grained olivine crystals. There are a few large low-Ca pyroxene crystals but not as a clear, continuous rim d) 1406-1, a porphyritic olivine-pyroxene chondrule, with a rim of coarse low-Ca pyroxenes, but distinct, coarse olivines in the core e) VIG6A, a porphyritic olivine-pyroxene chondrule, with low-Ca pyroxene more extensively replacing olivine throughout the chondrule f) MOK13B, a refractory olivine grain with inclusions of well-formed spinel (light green) and an irregular, fine grained intergrowth of diospide and anorthite (yellow).

Figure 4 $^{27}Al/^{24}Mg$ versus $\delta^{25}Mg$ for samples in this study a) subdivided according to meteorite b) compared to literature analyses (BIZZARRO et al., 2004; GALY et al., 2000; LUU et al., 2015; OLSEN et al., 2013; OLSEN et al., 2016; VAN KOOTEN et al., 2015; BOUVIER et al., 2013). Uncertainties shown in a) represent the 2sd reproducibility of JP-1 stock (see Table 2). For clarity error bars are not plotted in b), but typically 2se<0.05‰. To enable detail to be resolved in b), 4 chondrules with the most extreme $^{27}Al/^{24}Mg$ (>1.2) are not plotted. Dashed lines represent endmember mixing scenarios of chondritic composition ($^{27}Al/^{24}Mg$ = 0.1, $\delta^{25}Mg$ = -

0.12‰) with CAIs. Namely, admixtures with CAI material will move chondrule compositions to the right of the diagram between the bounds of the dashed lines. Notably some Al-rich chondrules (as identified by authors and indicated by the absence black lines around their symbols) populate this part of the diagram. However, other processes can also generate compositions in this field and in itself the diagram is not diagnostic (its use in conjunction with Fig. 7 provides clearer constraints).

Figure 5 $^{27}Al/^{24}Mg$ versus $\Delta'^{26}Mg$, isochron diagram, for the high precision analyses of CV chondrules and matrix in this study (filled circles) and (OLSEN et al., 2016), (open circles). Samples from different meteorites are indicated according to colour. Additionally the relict grain, Al-rich and matrix samples are identified. The horizontal shaded band shows an estimate of 'bulk chondrule' composition inferred from the weighted average of three chondrules with solar $^{27}Al/^{24}Mg$ (see text for further discussion). The solid grey dashed line is a canonical CAI array, using the slope of Jacobsen et al. (2008) passing through the 'chondrule reservoir' composition. The dashed blue line and dashed black lines are 'isochrons' with $(^{26}Al/^{27}Al)_0$ of $2x10^{-5}$ and $0.76x10^{-6}$ respectively (or 1Ma and 2Ma post CAI for a canonical, solar system initial as represented by the grey line) that pass through the 'chondrule reservoir' pivot point.

Figure 6 Model $(^{26}Al/^{27}Al)_0$ of individual chondrules from this study (filled blue circles) and selected literature data from *in situ*, internal isochrons; CV Allende (LUU et al., 2015), other CV (ferromagnesian chondrules from Ningqiang (HSU et al., 2003) with symbol border, Al-rich chondrules from Efremovka (HUTCHEON et al., 2009) without symbol border), CO3.05 Y81020 (KURAHASHI et al., 2008), LL3.0 Semarkona (VILLENEUVE et al., 2009) together with maximum values for Semarkona (RUSSELL et al., 1997) and LL3.1 Bishunpur (MOSTEFAOUI et al., 2002). The literature data were chosen to compare with existing CV data and show more extensive studies, and the highest values, obtained for primitive members of other meteorite groups.

Figure 7 $\delta^{25}Mg$ versus $\Delta'^{26}Mg$ a) for samples of this study (filled blue circles) compared to more extreme values reported for bulk CV chondrules (BIZZARRO et al., 2004; GALY et al., 2000), other literature bulk chondrule analyses (open diamonds, see references in Fig. 4) and CAI (green filled squares (BIZZARRO et al., 2004; GALY et al., 2000; JACOBSEN et al., 2008; LARSEN et al., 2011; MISHRA AND CHAUSSIDON, 2014; THRANE et al., 2006; WASSERBURG et al., 2012)). Dashed lines indicate mixing between a bulk chondritic composition (as defined by 'chondrule reservoir') and extreme CAI compositions, as can be seen more completely in b). The

most radiogenic ferromagnesian samples of this study are highlighted and do not show associated elevated δ^{25}Mg as predicted in most CAI mixing scenarios and is evident in Al-rich chondrules of this and previous work. Samples plausibly explained with a CAI contribution are indicated with white dashes. The composition of a putative condensate from a chondrule reservoir vapour, using a fractionation factor of 0.991 (RICHTER et al, 2008) is indicated with a grey cross. Interaction of chondrules with silicate vapour should trend towards such a composition.

Figure 8 $^{27}Al/^{24}Mg$ versus $\Delta'^{26}Mg$ for all literature data on bulk chondrules. The highest $^{27}Al/^{24}Mg$ samples are Al-rich chondrules from Allende (BIZZARRO et al., 2004; GALY et al., 2000; LUU et al., 2015). The errors for $^{27}Al/^{24}Mg$ are omitted (typically 5% or better), whilst those for $\Delta'^{26}Mg$ are quite variable and where not evident are smaller than the symbol. The two reference lines pass through the CV chondrule reservoir value with canonical CAI $(^{26}Al/^{27}Al)_0$ (JACOBSEN et al., 2008), solid line, and $(^{26}Al/^{27}Al)_0 = 2x10^{-5}$, dashed line. The white dashes mark the same samples identified in Fig. 7 whose compositions could plausibly be explained with a CAI component (the Al-rich chondrules of LUU et al, 2015 had no associated δ^{25}Mg and so cannot be similarly assessed).

Appendix 1 SEM images and element maps of all chondrules analysed in this study.

Appendix 2 Electron microprobe analyses of phases from the chondrule of this study.

References:

Alexander, C. M. O., Grossman, J. N., Ebel, D. S., and Ciesla, F. J., 2008. The formation conditions of chondrules and chondrites. *Science* **320**, 1617-1619.

Baker, J., Bizzarro, M., Wittig, N., Connelly, J., and Haack, H., 2005. Early planetesimal melting from an age of 4.5662 Gyr for differentiated meteorites. *Nature* **436**, 1127-1131.

Bizzarro, M., Baker, J. A., and Haack, H., 2004. Mg isotope evidence for contemporaneous formation of chondrules and refractory inclusions. *Nature* **431**, 275-278.

Bizzarro, M., Baker, J. A., Haack, H., and Lundgaard, K. L., 2005. Rapid timesclaes for accretion and melting of differentiated planetesimals inferred from ^{26}Al-^{26}Mg chronometry. *Astrophys. J.* **632**, L41-L44.

Bizzarro, M., Paton, C., Larsen, K., Schiller, M., Trinquier, A., and Ulfbeck, D., 2011. High precision Mg-isotope measurements of terrestrial and extraterrestrial material by HR-MC-ICMPS- implciation for the relative and absolute Mg-isotope composition of the bulk silicate Earth. *J. Anal. At. Spectrom.* **26**, 565-577.

Bollard, J., Connelly, J., and Bizzarro, M., 2015. Pb-Pb dating of individual chondrules from the CB_a chondrite Gujba: assessment of the impact plume formation model. *Meteorit. Planet. Sci.* **50**, 1197-1216.

Bollard. J., Connelly, J.N., Whitehouse, M.J., Pringle, E.A., Bonal, L., Jørgensen, J.K., Nordlund, Å. Moyneier, F., Bizzarro, M., 2017. Early formation of planetary building blocks inferred from Pb isotopic ages of chondrules. *Science Advances* **3**, e1700407

Bonal L., Quirico E., Bourot-Denise M., and Montagnac G. 2006. Determination of the petrologic type of CV3 chondrites by Raman spectroscopy of included organic matter. *Geochim. Cosmochim. Acta* **70**, 1849-1863.

Budde G., Kleine T., Kruijer T. S., Burkhardt C., and Metzler K. 2016. Tungsten isotopic constraints on the age and origin of chondrules. *Proc. Nat. Acad. Sci*. **113,** 2886-2891.

Bouvier, A., Wadhwa, M., Simon, S. B., and Grossman, L., 2013. Magnesium isotopic fractionation in chondrules from the Murchison and Murray CM2 carbonaceous chondrites. *Meteorit. Planet. Sci.* **48**, 339-353

Coath, C. D., Elliott, T., and Hin, R. C. (2017). Double spike inversion for three isotope systems. *Chem. Geol.* **451**, 78-89

Connelly, J. N., Bizzarro, M., Krot, A. N., Nordlund, A., Wielandt, D., and Ivanova, M. A., 2012. The absolute chronology and thermal processing of solids in the protoplanetary disk. *Science* **338**, 651-655.

Coplen, T. B., 2011. Guidelines and recommended terms for expression of stable-isotope-ratio and gas-ratio measurement results. *Rapid Commun. Mass Spectrom.* **25**, 2538-2560.

Friend, P., Hezel, D. C., and Mucerschi, D., 2016. The conditions of chondrule formation, Part II: Open system. *Geochim. Cosmchim. Acta* **173**, 198-209.

Galy, A., Yoffe, O., Janney, P. E., Williams, R. W., Cloquet, C., Alard, O., Halicz, L., Wadhwa, M., Hutcheon, I. D., Ramon, E., and Carigan, J., 2003. Magnesium isotope heterogeneity of the isotopic standard SRM980 and new reference materials for magnesium-isotope-ratio measurements. *J. Anal. At. Spectrom.* **18**, 1352-1356.

Galy, A., Young, E. D., Ash, R. D., and O'Nions, R. K., 2000. The formation of chondrules at high gas pressures in the solar nebula. *Science* **290**, 1751-1753.

Gounelle, M., Young, E. D., Shahar, A., Tonui, E., and Kearsley, A., 2007. Magnesium isotopic constraints on the origin of CB_b chondrites. *Earth Planet. Sci. Lett.* **256**, 521-533.

Hsu, W., Huss, G. R., and Wasserburg, G. J., 2003. Al-Mg systematics of CAIs, POI and ferromagnesian chondrules from Ningqiang. *Meteorit. Planet. Sci.* **38**, 35-48.

Hutcheon, I. D., Marhas, K. K., Krot, A. N., Goswami, J. N., and Jones, R. H., 2009. ^{26}Al in plagioclase-rich chondrules in carbonaceous chondrites: evidence for an extended duration of chondrule formation. *Geochim. Cosmochim. Acta* **73**, 5080-5099.

Imai, N., Terashima, S., Itoh, S., and Ando, A., 1995. 1994 compilation values for GSJ reference samples, "Igneous rock series". *Geochem. J.* **29**, 91-95.

Jacobsen, B., Yin, Q.-Z., Moynier, F., Amelin, Y., Krot, A. N., Nagashima, K., Hutcheon, I. D., and Palme, H., 2008. ^{26}Al-^{26}Mg and ^{207}Pb-^{206}Pb systematics of Allende CAIs: canonical solar initial ^{26}Al/^{27}Al ratio reinstated. *Earth Planet. Sci. Lett.* **272**, 353-364.

Jones, R. H., 1992. On the relationship between isolated and chondrule olivine grains in the carbonaceous chondrite ALHA77307. *Geochim. Cosmochim. Acta* **56**, 467-482.

Jones, R. H., Grossman, J. N., and Rubin, A. E., 2005. Chemical, mineralogical and isotopic properties of chondrules: clues to their origin. *In: Krot, A. N., Scott, E. R. D., and Reipurth, B. Eds.*), Chondrites and the Protoplanetary Disk.

Jones, R. H. and Schilk, A. J., 2009. Chemistry, petrology and bulk oxygen isotope composiitons of chondrules from the Mokoia CV3 carbonaceous chondrite. *Geochim. Cosmochim. Acta* **73**, 5854-5883.

Kita, N. T. and Ushikubo, T., 2012. Evolution of protoplanetary disk infered from ^{26}Al chronology of individual chondrules. *Meteorit. Planet. Sci.* **47**, 1108-1119.

Kita, N. T., Yin, Q.-Z., MacPherson, G. J., Ushibuko, T., Jacobsen, B., Nagashima, K., Kurahashi, E., Krot, A. N., and Jacobsen, S. B., 2013. ^{26}Al-^{26}Mg isotope systematics of the first solids in the early solar system. *Meteorit. Planet. Sci.* **48**, 1383-1400.

Krot, A. N., Amelin, Y., Cassen, P., and Meibom, A., 2005. Young chondrules in CB chondrites formed by a giant impact in the early Solar System. *Nature* **436**, 989-992.

Krot, A. N., Scott, E. R. D., and Zolensky, M., 1995. Mineralogical and chemical modification of components in CV3 chondrites: nebular or asteroidal processing? *Meteoritics* **30**, 748-775.

Kurahashi, E., Kita, N. T., Nagahara, H., and Morishita, Y., 2008. ^{26}Al-^{26}Mg systematics of chondrules in a primitive CO chondrite. *Geochim. Cosmochim. Acta* **72**, 3865-3882.

Larsen, K. K., Trinquier, A., Paton, C., Schiller, M., Wielandt, D., Ivanova, M. A., Connelly, J. N., Nordlund, A., Krot, A. N., and Bizzarro, M., 2011. Evidence for magnesium isotope heteroegenity in the solar protoplaneary disk. *Astrophys. J.* **735** p. L37.

Larsen, K. K., Schiller, M., Bizzarro M., 2016. Accretion timescales and style of asteroidal differentiation in an ^{26}Al-poor protoplanetary disk. *Geochim. Cosmochim. Acta*, **176** 295-315

Libourel, G., Krot, A. N., and Tissander, L., 2006. Role of gas-melt interaction during chondrule formation. *Earth Planet. Sci. Lett.* **251**, 232-240.

Luu, T.-H., Young, E. D., Gounelle, M., and Chaussidon, M., 2015. Short time interval for condensation of high-temperature silicates in the solar accretion disk. *Proc. Natl. Acad. Sci* **112**, 1298-1303.

Makishima, A. and Nakamura, E., 2000. Determination of titanium at μg g^{-1}levels in milligram amounts of silicate materials by isotope dilution high resolution inductively coupled plasma mass spectrometry with flow injection. *J. Anal. At. Spectrom.* **15**, 263-267.

Marrochi, Y. and Chaussidon, M., 2015. A systematic for oxygen istopic variation in meteoritic chondrules. *Earth Planet. Sci. Lett.* **430**, 308-315.

Maruyama, S. and Yurimoto, H., 2003. Relationship among O, Mg isotopes and the petrology of two spinel-bearing compound chondrules. *Geochim. Cosmochim. Acta* **67**, 3943-3957.

McKeegan K.D, Leshin L.A, Russell S.S, MacPherson G.J, 1998. Oxygen isotopic abundances in calcium-aluminum-rich inclusions from ordinary chondrites: Implications for nebular heterogeneity. *Science*, **280** 414-418

Mishra, R. K. and Chaussidon, M., 2014. Timing and extent of Mg and Al isotopic homogenization in the early inner Solar System. *Earth Planet. Sci. Lett.* **390**, 318-326.

Mostefaoui, S., Kita, N. T., Togashi, S., Tachibana, S., Nagahara, H., and Morishita, Y., 2002. The relative formation ages of ferromagnesian chondrules inferred from their inital aluminum-26/aluminium-27 ratios. *Meteorit. Plan. Sci.* **37**, 421-438.

Nagahara H., Kita N. T., Ozawa K., and Morishita Y. 1999. Condensation during chondrule formation: Elemental and Mg isotopic evidence. *30th Lunar Planet. Sci. Conf*. #1917 (abstract).

Olsen, M., Schiller, M., Krot, A. N., and Bizzarro, M., 2013. Magnesium isotope evidence for single stage formation of CB chondrules by colliding planetesimals. *Astrophys. J. Lett.* **776**, L1.

Olsen, M., Wielandt, D., Schiller, M., van Kooten, E. M. M. E., and Bizzarro, M., 2016. Magnesium and ^{54}Cr isotope compositions of carbonaceous chondrite chondrules- insights into early disk processes. *Geochim. Cosmochim. Acta* **191**, 118-138.

Pack, A., Yurimoto, H., and Palme, H., 2004. Petrographic and oxygen-isotopic study of refractory forsterites from R-chondrites Dar al Gani (R3.5-6), unequilibrated ordinary and carbonaceous chondrites. *Geochim. Cosmochim. Acta* **68**, 1135-1157.

Palme, H., Hezel, D. C., and Ebel, D. S., 2015. The origin of chondrules: constraints from matrix composition and matrix-chondrule complementarity. *Earth Planet. Sci. Lett*. **411**, 11-19.

Pogge von Strandmann, P. A. E., 2008. Precise magnesium isotope measurements in core top planktic and benthic foraminifera. Geochim. Geophys. Geosyst. 9, Q12015, doi:10.1029/2008GC002209.

Pogge von Strandmann, P. A. E., Elliott, T., Marschall, H., Coath, C. D., Lai, Y.-J., Jeffcoate, A. B., and Ionov, D., 2011. Variations of Li and Mg isotope ratios in bulk chondrites and mantle xenoliths. *Geochim. Cosmochim. Acta* **75**, 5247-5268.

Regelous, M., Elliott, T., and Coath, C. D., 2008. Nickel isotope heterogeneity in the early Solar System. *Earth Planet. Sci. Lett.* **272**, 330-338.

Richter, F. M., Janney, P. E., Mendybaev, R. A., Davis, A. M., and Wadhwa, M., 2007. Elemental and isotopic fractionation of Type B CAI-like liquids by evaporation. *Geochim. Cosmochim. Acta* **71**, 5544-5564.

Russell, S. S., Huss, G. R., MacPherson, G. J., and Wasserburg, G. J., 1997. Early and late chondrule formation: new constraints for solar nebula chronology from ^{26}Al/^{27}Al in unequilibrated ordinary chondrites. *Lunar Planet. Sci.* **28**, 1468.

Russell, S. S., Krot, A. N., Huss, G. R., Keil, K., Itoh, S., Yurimoto, H., and MacPherson, G. J., 2005. The genetic relationship between refractory inclusons and chondrules. *In: Krot, A. N., Scott, E. R. D., and Reipurth, B. Eds.*), Chondrites and the Protoplanetary Disk.

Scott, E. R. D., Jones, R. H., and Rubin, A. E., 1994. Classification, metamorphic history and pre-metamorphic composition of chondrules. *Geochim. Cosmochim. Acta* **58**, 1203-1209.

Schiller, M., Handler, M. R., and Baker, J. A., 2010. High-precision Mg isotopic systematics of bulk chondrites. *Earth Planet. Sci. Lett*. **297**, 165-173.

Schiller, M., Connelly, J.N., Glad, A.C., Mikouchi, T., Bizzarro, M., 2015. Early accretion of protoplanets inferred from a reduced inner solar system ^{26}Al inventory. *Earth Planet. Sci. Lett*. **420**, 45–54

Shu, F. H., Shang, H., and Lee, T., 1996. Toward an astrophysical theory of chondrites. *Science* **271**, 1545-1552.

Stracke, A., Palme, H., Gellissen, M., Münker, C., Kleine, T., Birbaum, K., Günther, D., Bourdon, B., and Zipfel, J., 2012. Refractory element fractionation in the Allende meteorite: implications for solar nebula condesnation and the chondrite composition of planetary bodies. *Geochim. Cosmochim. Acta* **85**, 114-141.

Tachibana, S., Nagahara, H., Mostefaoui, S., and Kita, N. T., 2003. Correlation between relative ages inferred from ^{26}Al and bulk composiitons of ferromagnesian chondrules in least equilbrated ordinary chondrites. *Meteorit. Planet. Sci.* **38**, 939-962.

Teng, F.-Z., Wadhwa, M., and Helz, R. T., 2007. Investigation of magnesium isotope fractionation during basalt differentiation: implications for a chondritic composition of the terrestrial mantle. *Earth Planet. Sci. Lett.* **261**, 84-92.

Teng, F. Z., Li, W. Y., Ke, S., Marty, B., Huang, S. C., Wu, F. Y., and Pourmand, A., 2010. Magnesium isotopic composition of the Earth and chondrites. *Geochim. Cosmochim. Acta* **74**, 4150-4166.

Thrane, K., Bizzarro, M., and Baker, J. A., 2006. Extremely brief formation interval for refractory inclusions and uniform distribution of Al-26 in the early solar system. **646**, L159-L162.

Tissander, L., Libourel, G., and Robert, F., 2002. Gas-melt interactions and their bearing on chondrule formation. *Meteorit. Planet. Sci.* **37**, 1377-1389.

Tomeoka K. and Ohnishi I. (2014) Olivine-rich rims surrounding chondrules in the Mokoia CV3 carbonaceous chondrite: further evidence for parent-body processes. *Geochim. Cosmochim. Acta*, **137** 18-34

Trinquier, A., Elliott, T., Ulfbeck, D., Coath, C., Krot, A. N., and Bizzarro, M., 2009. Origin of nucleosynthetic isotope heterogeneity in the solar protoplanetary disk. *Science* **324**, 374-376.

Ushikubo T., Nakashima D., Kimura M., Tenner T. J., and Kita N. T. (2013) Contemporaneous formation of chondrules in distinct oxygen isotope reservoirs. *Geochim. Cosmochim. Acta* **109**, 280-295.

van Kooten, E. M. M. E., Wielandt, D., Schiller, M., Nagashima, K., Thomen, A., Larsen, K. K., Olsen, M. B., Nordland, A., Krot, A. N., and Bizzarro, M., 2015. Isotopic evidence for primordial molecular cloud material in metal-rich carbonaceous chondrites. *Proc. Natl. Acad. Sci. USA* **113**, 2011-2016.

Victor, A. H., 1986. Separation of nicel from other elements by cation-exchange chromatography in dimehtylglyoxime/hydrochloric acid/acetone media. *Anal. Chim. Acta* **183**, 155-161.

Villeneuve, J., Chaussidon, M., and Libourel, G., 2009. Homogenous distribution of ^{26}Al in the solar system from the Mg isotopic composition of chondrules. *Science* **325**, 985-988.

Villeneuve, J., Chaussidon, M., and Libourel, G. (2012) Lack of relationship between 26Al ages of chondrules and their mineralogical and chemical compositions. *Comptes Rendus Geoscience* **344** 423-431.

Wasserburg, G. J., Wimpenny, J., and Yin, Q. Z., 2012. Mg isotopic heterogeneity, Al-Mg isochrons and canonical ^{26}Al/^{27}Al in the early solar system. *Meteorit. Planet. Sci.* **47**, 1980-1997.

Wasson J. T. and Kallemeyn G. 1998. The Solar System: chemistry as a key to its origin - Compositions of chondrites. *Phil. Trans. Royal Soc.* A. **325** 535-544.

Young, E. D. and Galy, A., 2004. The isotope geochemistry and cosmochemistry of magnesium. *In: Johnson, C. M., Beard, B. L., and Albarède, F. Eds.*), Geochemistry of non-traditional stable isotopes. Mineralogical Society of America, Washington, D.C.

Sample	Meteorite	Batch	Petrographic type	Weight (mg)	Ti/Mg (wt/wt)	Na/Mg (wt/wt)	Ni/Mg (wt/wt)	Fe/Mg (wt/wt)	$^{27}Al/^{24}Mg$ (atomic)
YJ10	Mokoia	1	Al-rich	2.35	0.0238	0.0589	0.0383	0.542	0.371
YJ8	Mokoia	1	POP	6.4	0.0054	0.0119	0.0495	0.649	0.108
YJ9	Mokoia	1	POP	1.8	0.0030	0.0118	0.0066	0.171	0.041
MOK1	Mokoia	2	POP	0.63	0.0052	0.0193	0.0111	0.220	0.108
MOK2	Mokoia	2	POP	1.13	0.0165	0.0481	0.0575	0.739	0.286
MOK3	Mokoia	2	POP	0.95	0.0084	0.0603	0.0413	0.421	0.197
MOK4	Mokoia	2	POP	0.53	0.0154	0.0470	0.0382	0.449	0.218
MOK5	Mokoia	2	POP	1.03	0.0077	0.0271	0.0249	0.451	0.162
MOK13B	Mokoia	3	PO	0.32	0.0055		0.0091	0.179	0.028
YJ3	Vigarano	1	POP	1.28	0.0060	0.0122	0.0567	0.649	0.125
VIG1	Vigarano	2	POP	0.74	0.0110	0.0356	0.0359	0.528	0.202
VIG2	Vigarano	2	POP	0.91	0.0147	0.0402	0.0417	0.601	0.271
VIG1A	Vigarano	3	POP	1.49	0.0080	0.0184	0.0780	0.718	0.161
VIG6A	Vigarano	3	POP	0.4	0.0041		0.0651	0.908	0.058
1406-1	Vigarano	3	POP	1.03	0.0110	0.0285	0.0372	0.554	0.209
1406-3	Vigarano	3	POP	0.49	0.0046	0.0064	0.0182	0.449	0.035
1406-20	Vigarano	3	PP	0.85	0.0052	0.0078	0.0423	0.558	0.054
YJ4	Allende	1	BO	0.3	0.0064	0.0310	0.0148	0.235	0.134
YJ5	Allende	1	POP	0.85	0.0052	0.0321	0.0203	0.372	0.100
YJ6	Allende	1	POP	0.86	0.0047	0.0155	0.0395	0.514	0.089
YJ7	Allende	1	PO	0.67	0.0005	0.0057	0.0026	0.655	0.009
JP-1/2		2					0.00873	0.212	0.01555
JP-1/3		3			0.00009	0.00063	0.00941	0.215	0.01450
JP-1 reference					0.00007	0.00058	0.00914	0.217	0.01484

Table 1

Sample	$^{27}Al/^{24}Mg$ (atomic)	$\delta^{25}Mg$ ‰	±2se	n	$\delta^{25}Mg$ (DS) ‰	$\Delta'^{26}Mg$ ppm	±2se	n
YJ10	0.371	*0.240*	*0.009*	20		44.2	3.5	20
YJ8	0.108	*-0.117*	*0.011*	16		8.6	3.9	16
YJ9	0.041	*-0.180*	*0.008*	16		-2.5	3.9	16
MOK1	0.108	-0.034	0.009	32		-1.0	2.8	32
MOK2	0.286	-0.099	0.011	28		16.2	3.0	28
MOK3	0.197	-0.050	0.008	26		10.3	3.4	26
MOK4	0.218	0.218	0.007	28		9.8	3.0	28
MOK5	0.162	0.089	0.008	26		8.5	3.2	26
MOK13B	0.028	-0.069	0.007	10	-0.110	-16.5	2.7	30
YJ3	0.125	*-0.059*	*0.013*	5		3.9	7.0	5
VIG1	0.202	-0.078	0.012	28	-0.118	16.6	3.0	28
VIG2	0.271	-0.127	0.009	33	-0.113	26.8	2.6	33
VIG1A	0.161	-0.021	0.014	12	-0.107	3.9	2.6	32
VIG6A	0.058	-0.067	0.011	10		0.0	2.7	30
1406-1	0.209	0.186	0.024	20	0.183	7.0	2.3	40
1406-3	0.035	-0.045	0.004	10		-0.3	2.5	35
1406-20	0.054	-0.077	0.007	10	-0.071	4.7	2.7	30
YJ4	0.134	*-0.271*	*0.017*	7		-1.2	5.9	7
YJ5	0.100	*-0.222*	*0.011*	14		3.2	4.2	14
YJ6	0.089	*-0.097*	*0.023*	16		7.9	3.9	16
YJ7	0.009	*-0.141*	*0.008*	23		5.9	3.3	23
JP-1_1		-0.123	0.013	28		0.2	3.4	28
JP-1c		-0.139	0.015	8		0.8	6.8	8
JP-1j						4.4	6	10
JP-1m						0.7	7.7	6
			±2sd					
JP-1 stock		-0.181	0.077	130		2.0	1.1	206
JP-1 mean						**1.9**	**1.0**	**258**
BHVO-2						-1.4	6	10
BIR						0.7	6	10

Table 2

Sample	Model $(^{26}Al/^{27}Al)_0$ x 10^{-5}	2se ±	Model Age (Ma post CAI)	2se +	2se -	Model Age (Ma post CAI)	Model Age (Ma post CAI)
YJ10	2.19	0.27	0.90	0.13	0.12	0.00	0.47
YJ9	1.10	0.96	*1.61*	*2.14*	*0.65*	0.72	1.18
MOK2	1.05	0.29	1.66	0.34	0.25	0.76	1.22
MOK3	1.18	0.62	1.54	0.76	0.43	0.64	1.10
MOK4	0.90	0.45	1.82	0.73	0.42	0.92	1.39
MOK5	1.46	0.96	1.32	1.11	0.52	0.42	0.89
MOK13B	3.44	0.66	0.43	0.22	0.18	-0.46	0.00
YJ3	1.00	5.18	*1.71*	*inf*	*1.88*	*0.82*	*1.28*
VIG1	2.02	0.57	0.98	0.34	0.26	0.09	0.55
VIG2	2.05	0.33	0.97	0.18	0.16	0.07	0.54
VIG1A	0.35	0.84	*2.80*	*inf*	*1.26*	*1.90*	*2.37*
VIG6A	0.75	1.00	*2.01*	*inf*	*0.87*	*1.11*	*1.57*
1406-1	0.60	0.42	2.24	1.25	0.55	1.35	1.81
1406-3	0.57	0.64	*2.29*	*inf*	*0.78*	*1.40*	*1.86*
			canonical $(^{26}Al/^{27}Al)_0$ $5.23x10^{-5}$			Olsen et al. 16 $(^{26}Al/^{27}Al)_0$ $2.2x10^{-5}$	MOK13B min. $(^{26}Al/^{27}Al)_0$ $3.4x10^{-5}$

Table 3

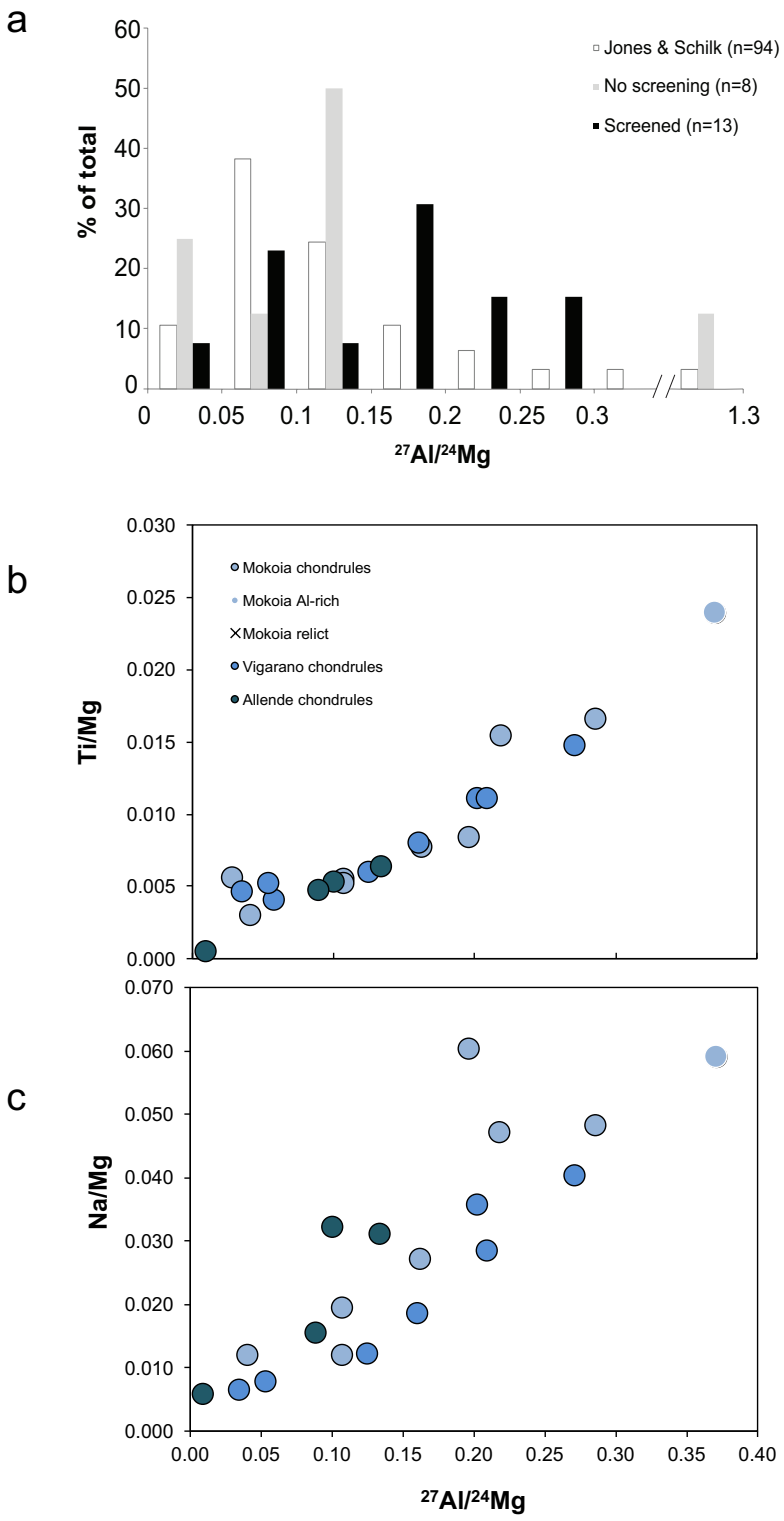
a
60
50
40
30
20
10
0
% of total
0
0.05
0.1
0.15
0.2
0.25
0.3
1.3
27Al/24Mg
Jones & Schilk (n=94)
No screening (n=8)
Screened (n=13)
b
0.030
0.025
0.020
0.015
0.010
0.005
0.000
Ti/Mg
Mokoia chondrules
Mokoia Al-rich
Mokoia relict
Vigarano chondrules
Allende chondrules
c
0.070
0.060
0.050
0.040
0.030
0.020
0.010
0.000
Na/Mg
0.00
0.05
0.10
0.15
0.20
0.25
0.30
0.35
0.40
27Al/24Mg

Figure 1

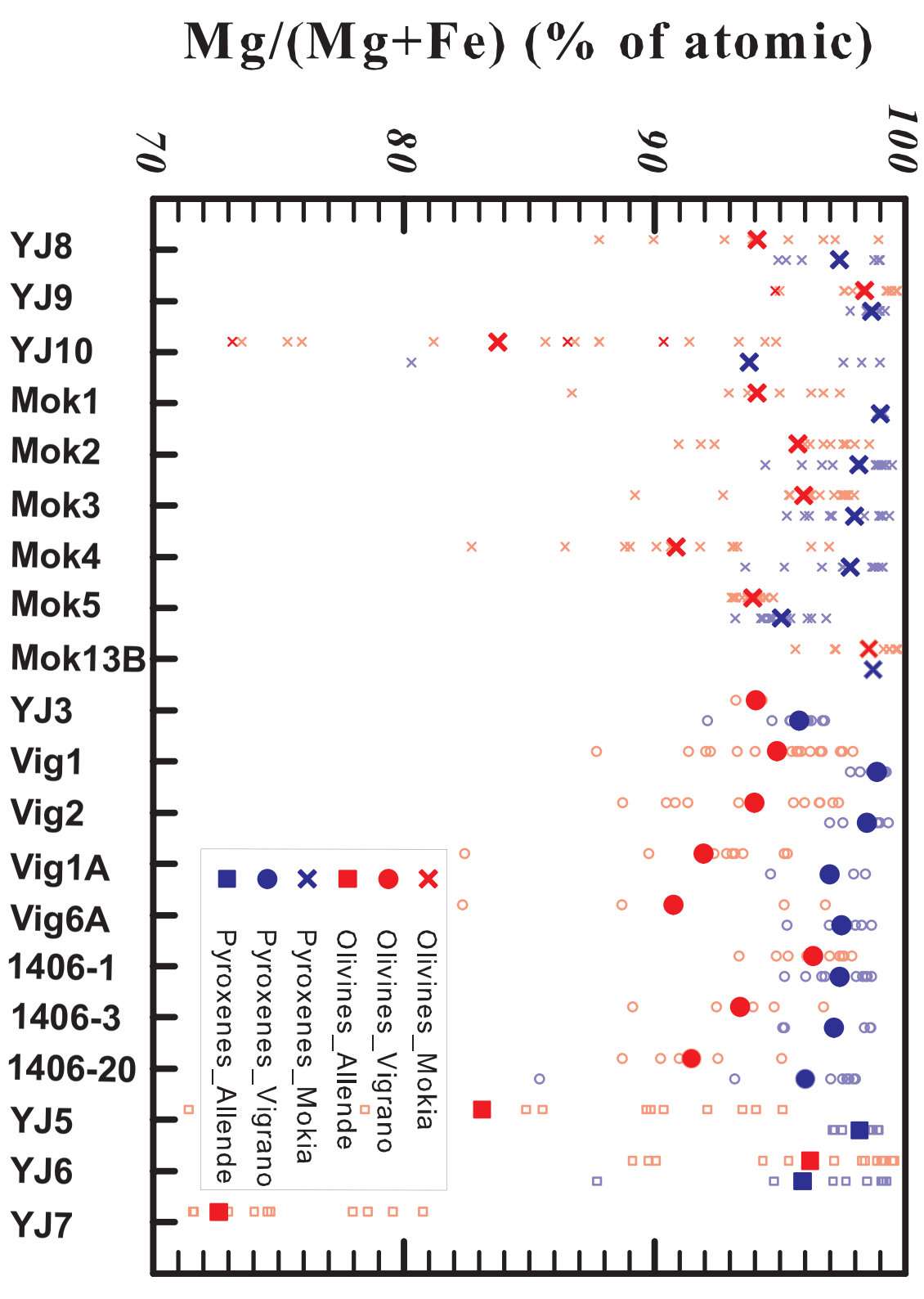
Mg/(Mg+Fe) (% of atomic)
70
80
90
100
YJ8
YJ9
YJ10
Mok1
Mok2
Mok3
Mok4
Mok5
Mok13B
YJ3
Vig1
Vig2
Vig1A
Vig6A
1406-1
1406-3
1406-20
YJ5
YJ6
YJ7
Olivines_Mokia
Olivines_Vigrano
Olivines_Allende
Pyroxenes_Mokia
Pyroxenes_Vigrano
Pyroxenes_Allende

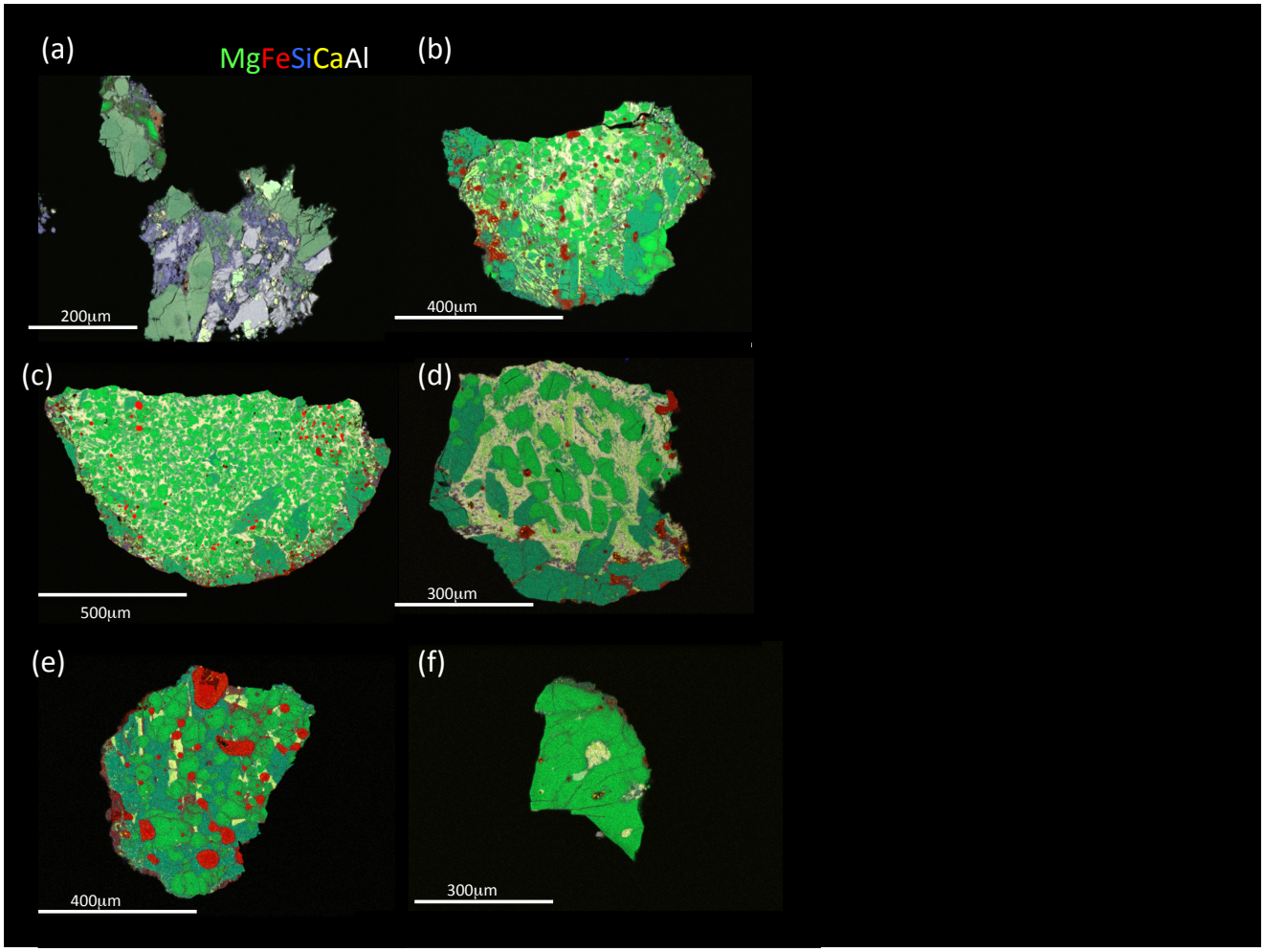
(a)
MgFeSiCaAl
200μm
(b)
400μm
(c)
500μm
(d)
300μm
(e)
400μm
(f)
300μm

a

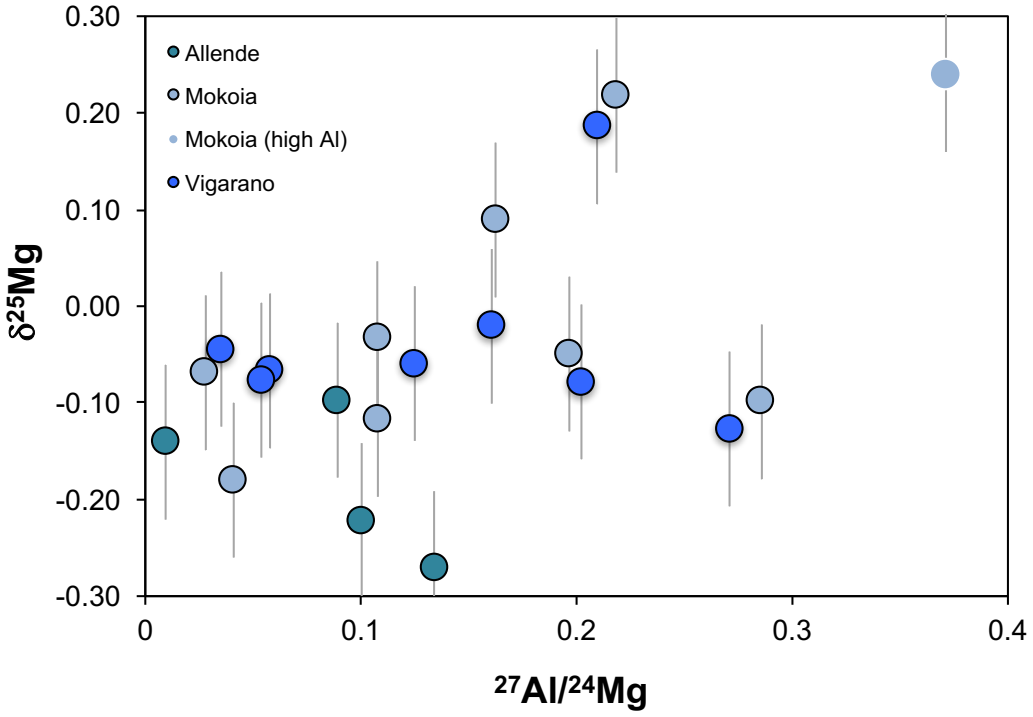
Allende
Mokoia
Mokoia (high Al)
Vigarano
δ25Mg
27Al/24Mg
0.30
0.20
0.10
0.00
-0.10
-0.20
-0.30
0
0.1
0.2
0.3
0.4

b

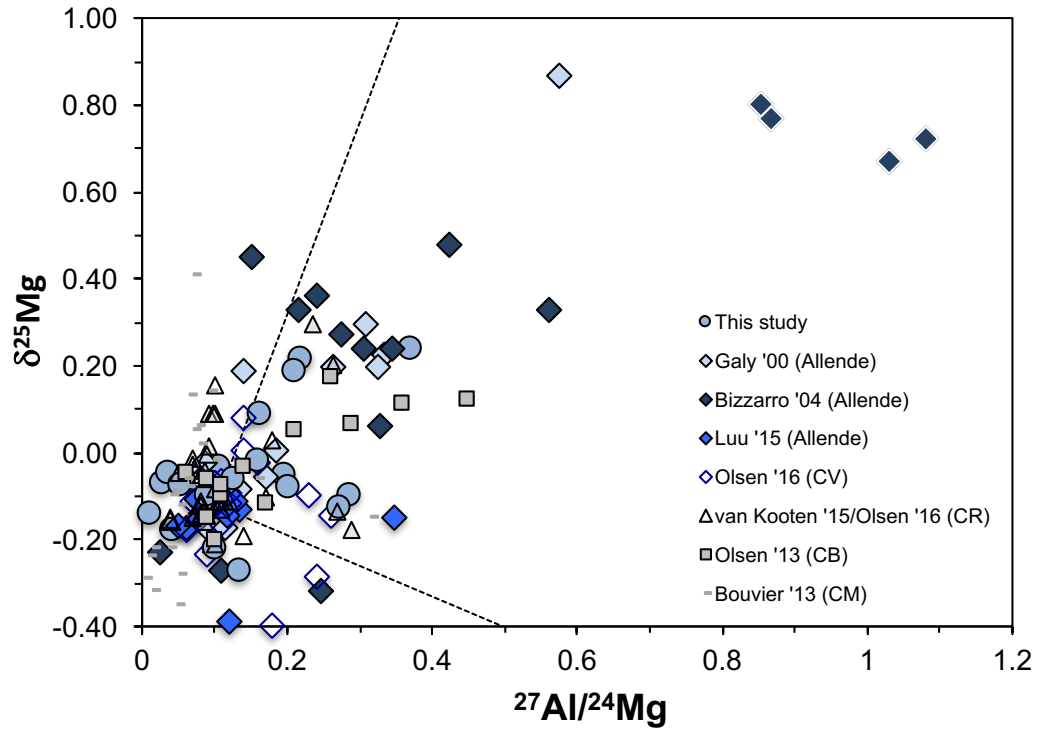
This study
Galy '00 (Allende)
Bizzarro '04 (Allende)
Luu '15 (Allende)
Olsen '16 (CV)
van Kooten '15/Olsen '16 (CR)
Olsen '13 (CB)
Bouvier '13 (CM)
δ25Mg
27Al/24Mg
1.00
0.80
0.60
0.40
0.20
0.00
-0.20
-0.40
0
0.2
0.4
0.6
0.8
1
1.2

Figure 4

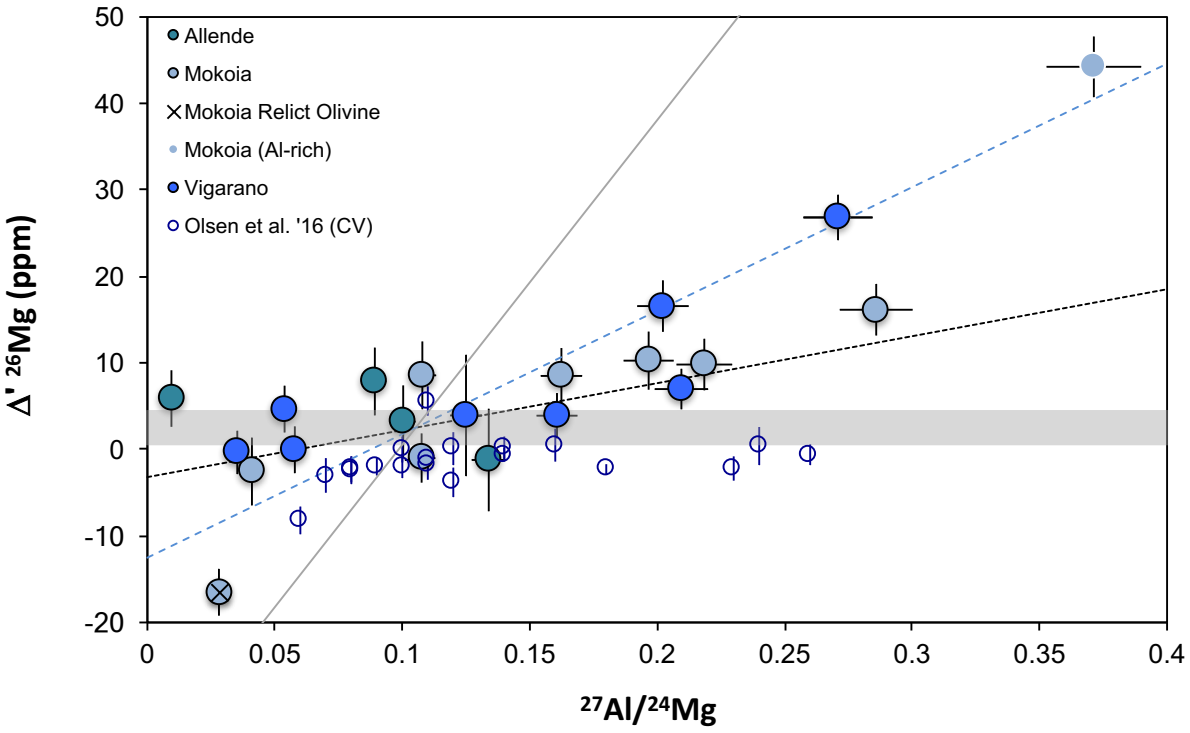
Allende
Mokoia
Mokoia Relict Olivine
Mokoia (Al-rich)
Vigarano
Olsen et al. '16 (CV)
Δ' 26Mg (ppm)
27Al/24Mg
50
40
30
20
10
0
-10
-20
0
0.05
0.1
0.15
0.2
0.25
0.3
0.35
0.4

Figure 5

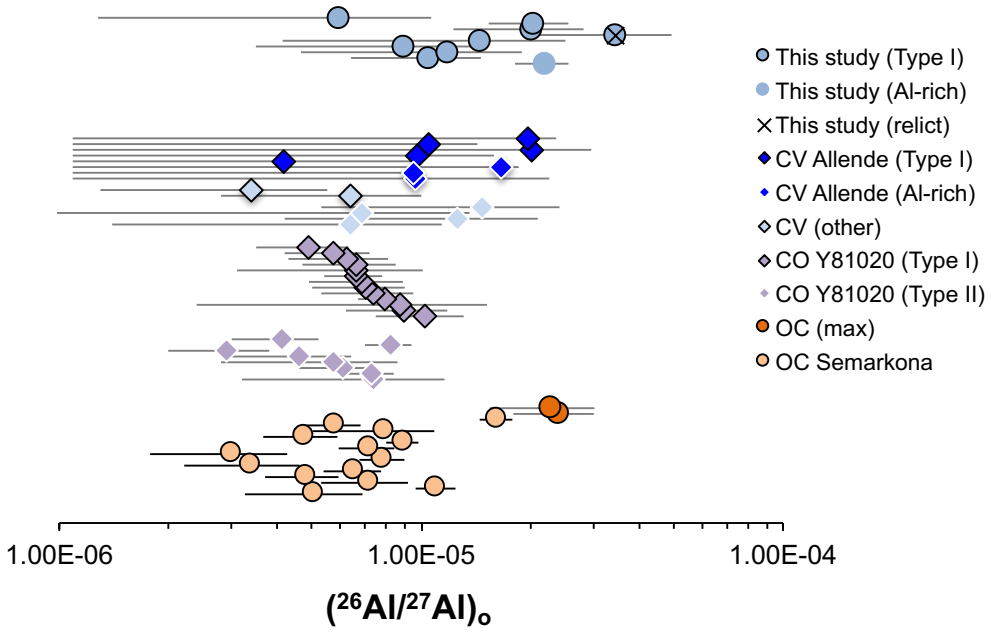
This study (Type I)
This study (Al-rich)
This study (relict)
CV Allende (Type I)
CV Allende (Al-rich)
CV (other)
CO Y81020 (Type I)
CO Y81020 (Type II)
OC (max)
OC Semarkona
1.00E-06
1.00E-05
1.00E-04
(26Al/27Al)o

Figure 6

a

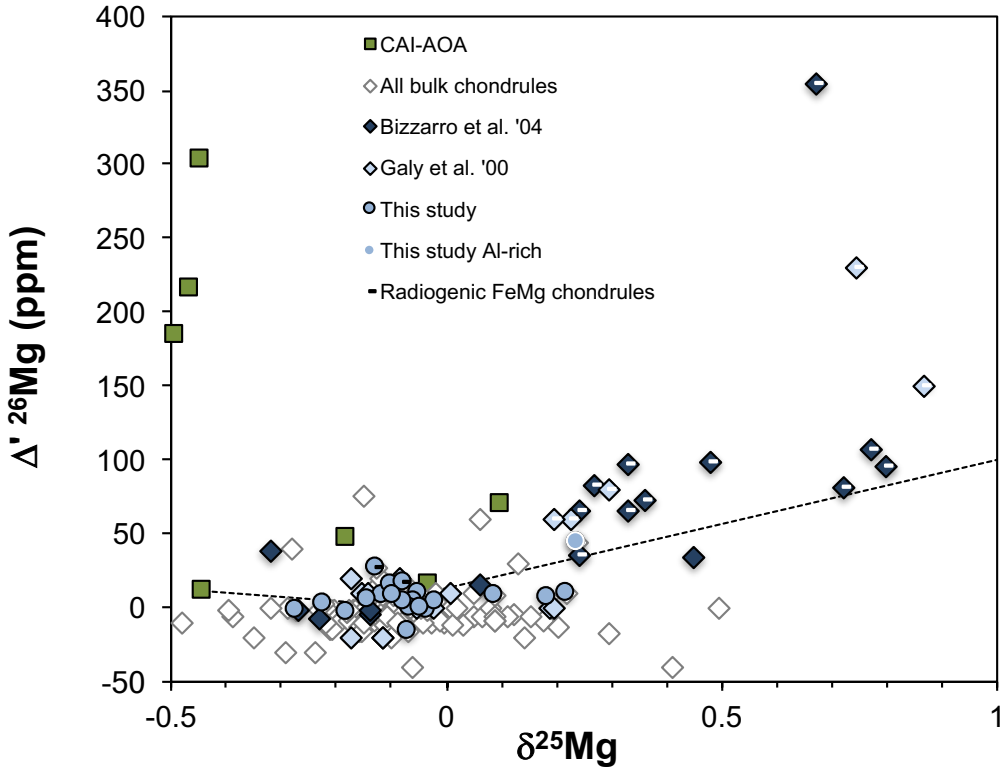
CAI-AOA
All bulk chondrules
Bizzarro et al. '04
Galy et al. '00
This study
This study Al-rich
Radiogenic FeMg chondrules
Δ' 26Mg (ppm)
δ25Mg
400
350
300
250
200
150
100
50
0
-50
-0.5
0
0.5
1

b

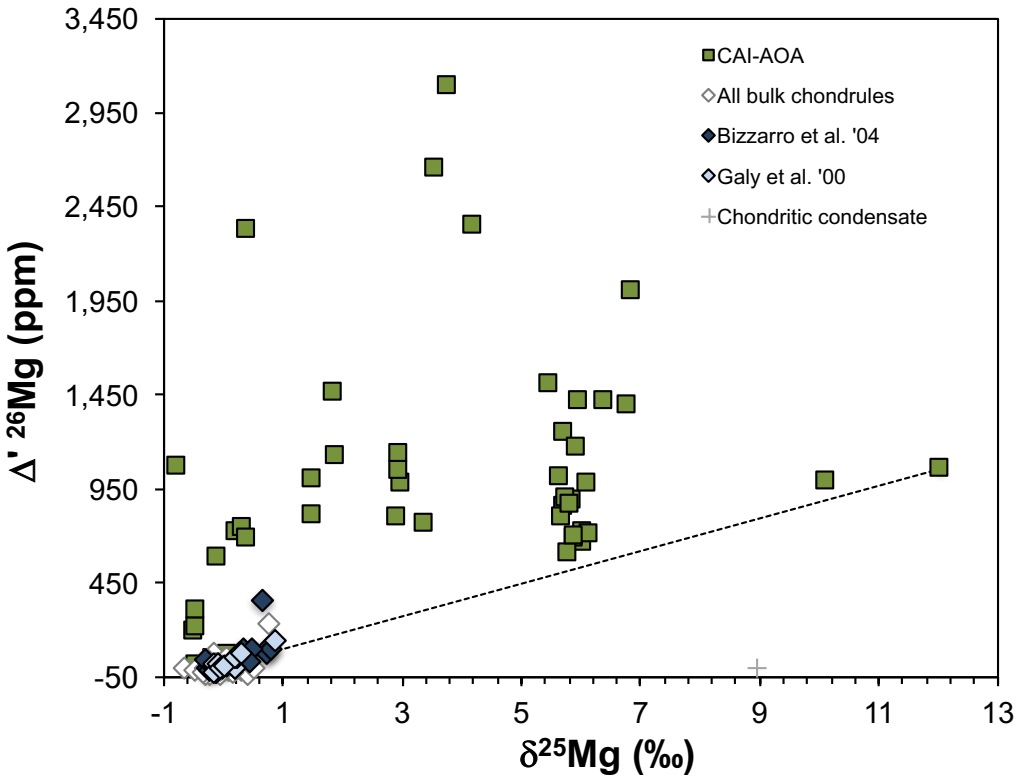
CAI-AOA
All bulk chondrules
Bizzarro et al. '04
Galy et al. '00
Chondritic condensate
Δ' 26Mg (ppm)
δ25Mg (‰)
3,450
2,950
2,450
1,950
1,450
950
450
-50
-1
1
3
5
7
9
11
13

Figure 7

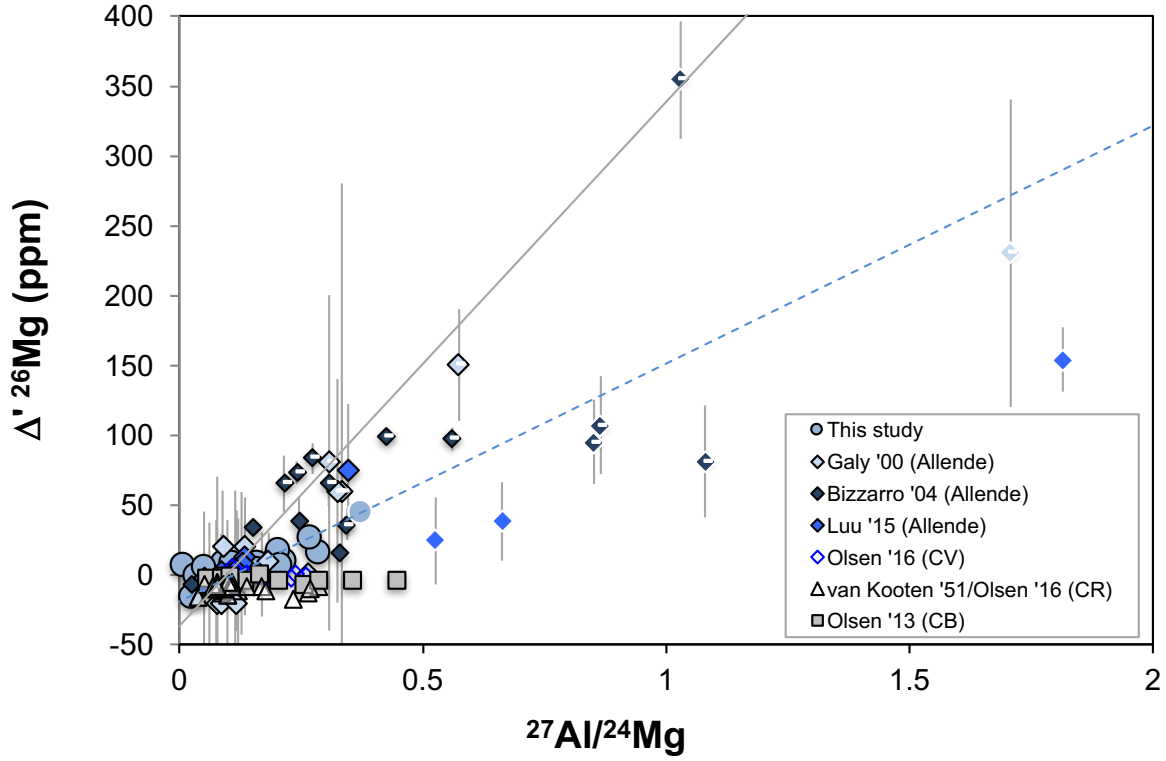
400
350
300
250
200
150
100
50
0
-50
0
0.5
1
1.5
2
Δ' 26Mg (ppm)
27Al/24Mg
This study
Galy '00 (Allende)
Bizzarro '04 (Allende)
Luu '15 (Allende)
Olsen '16 (CV)
van Kooten '51/Olsen '16 (CR)
Olsen '13 (CB)

Figure 8

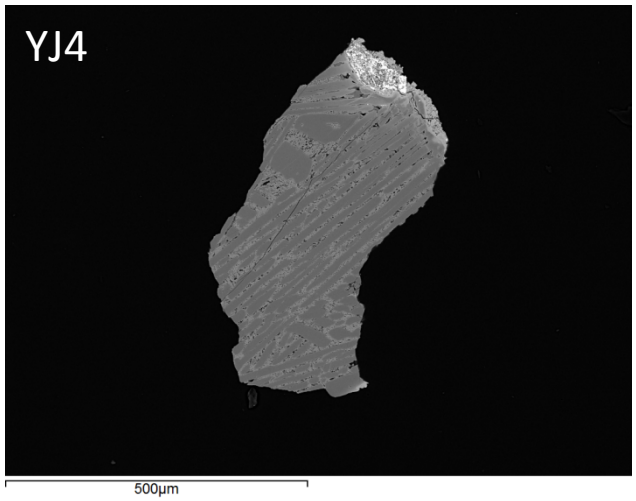
YJ4
500μm

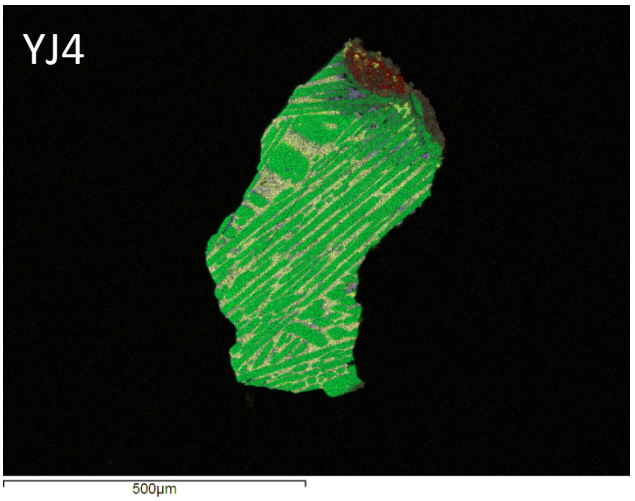
YJ4
500μm

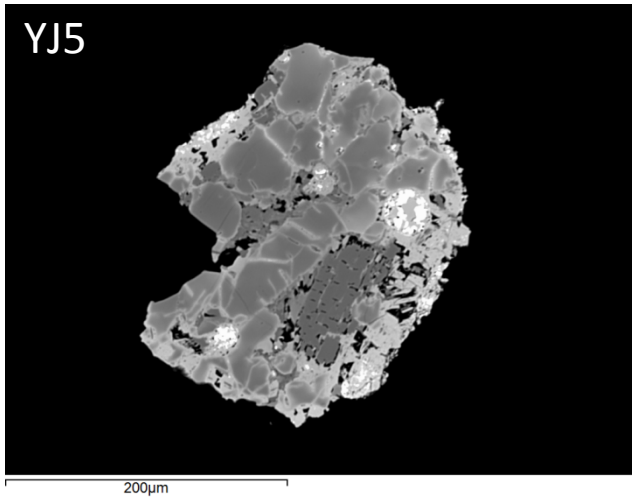
YJ5
200μm

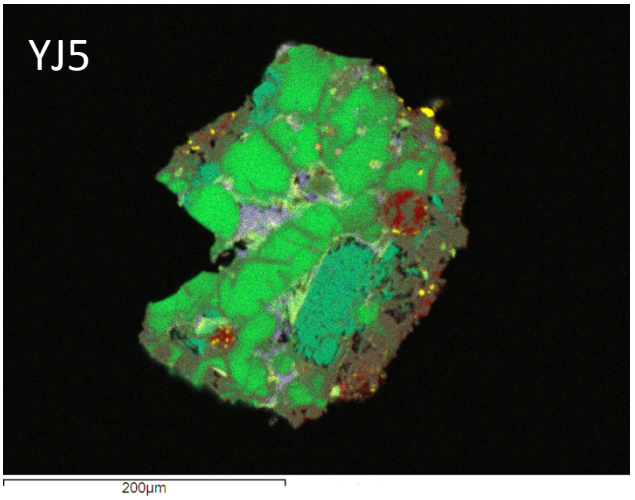
YJ5
200μm

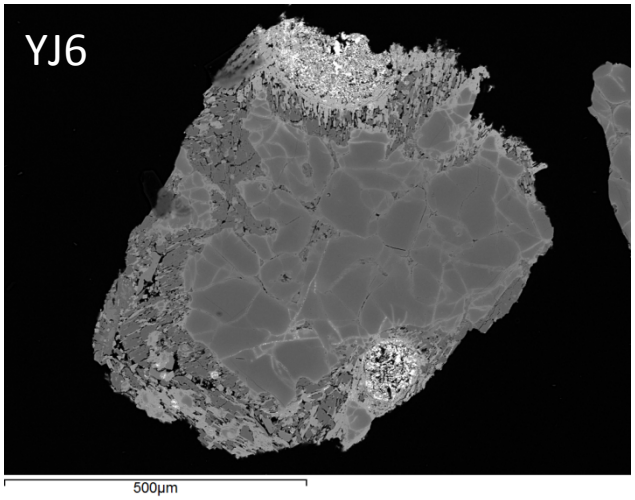
YJ6
500μm

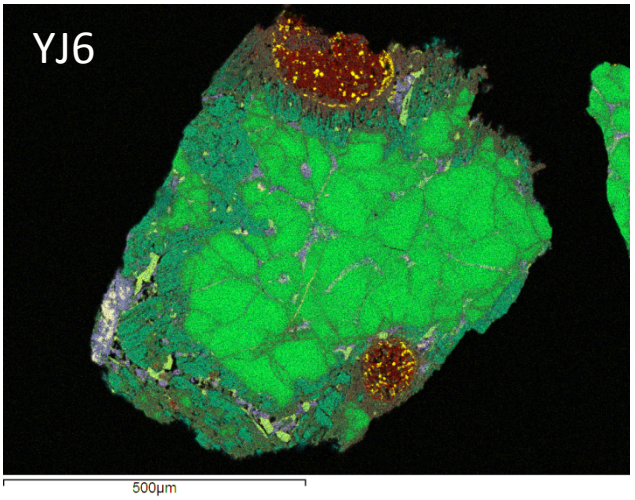
YJ6
500μm

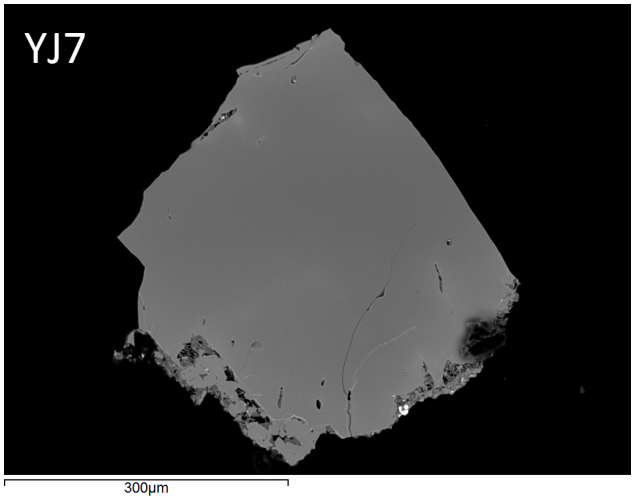
YJ7
300μm

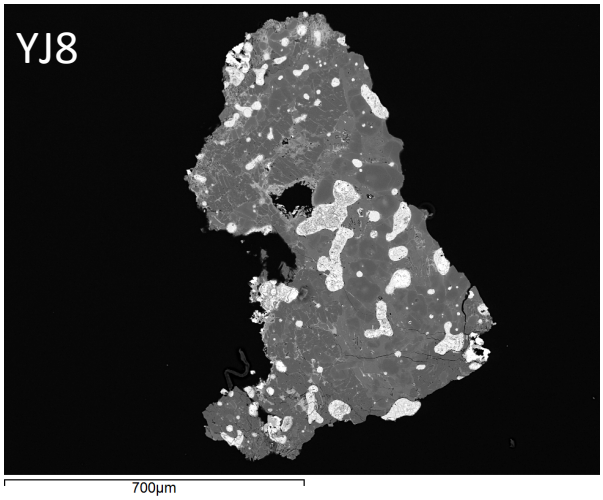
YJ8
700μm

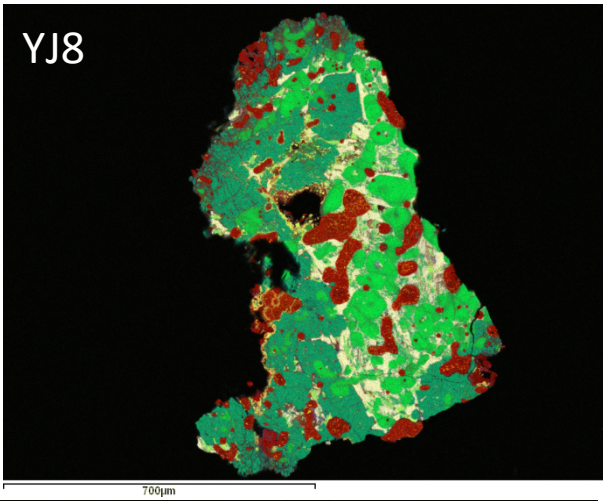
YJ8
700μm

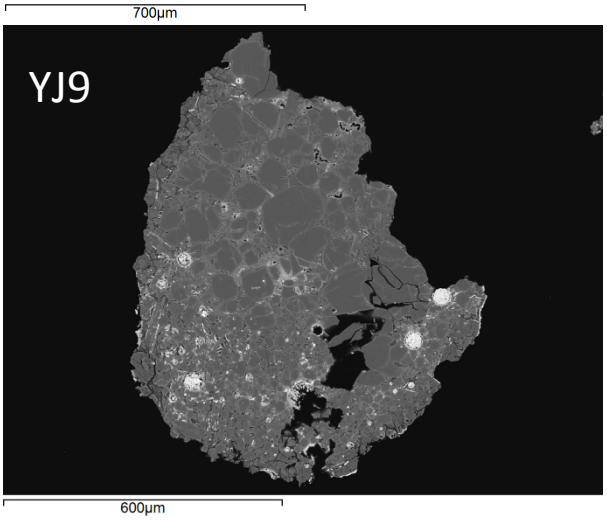
YJ9
600μm

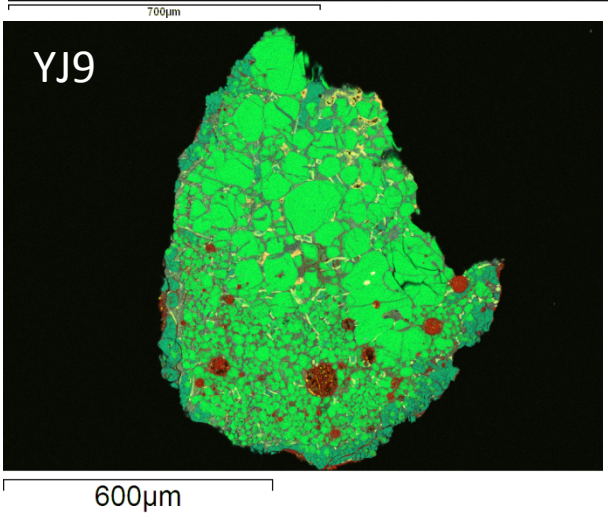
YJ9
600μm

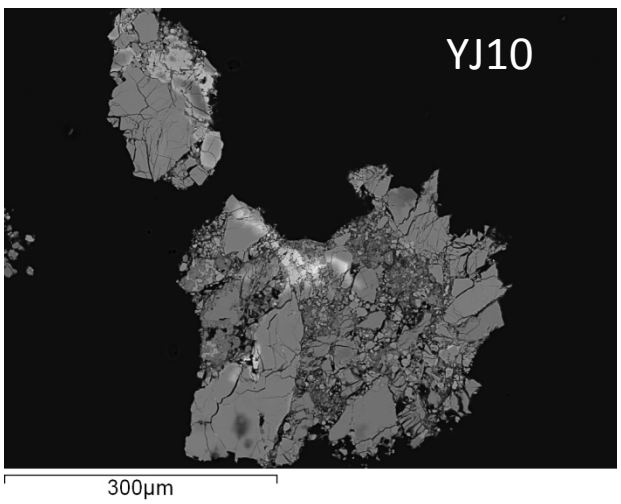
YJ10
300μm

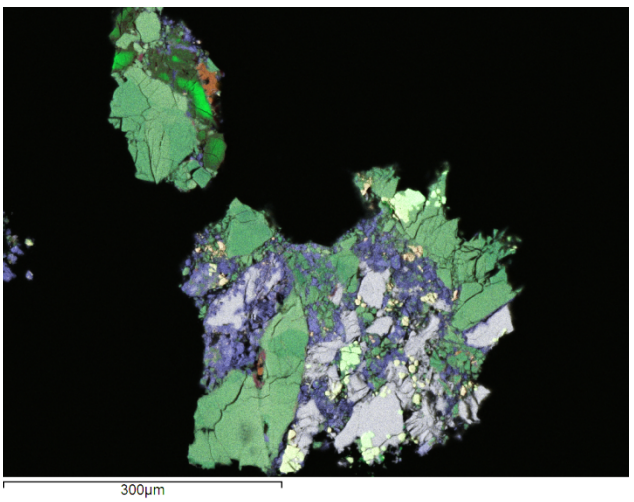
300μm

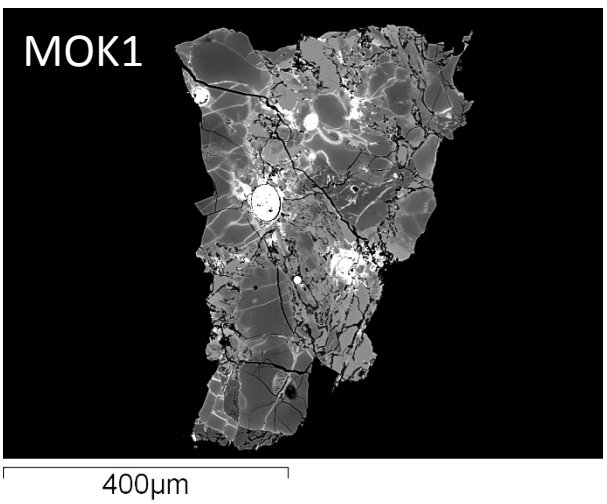
MOK1
400μm

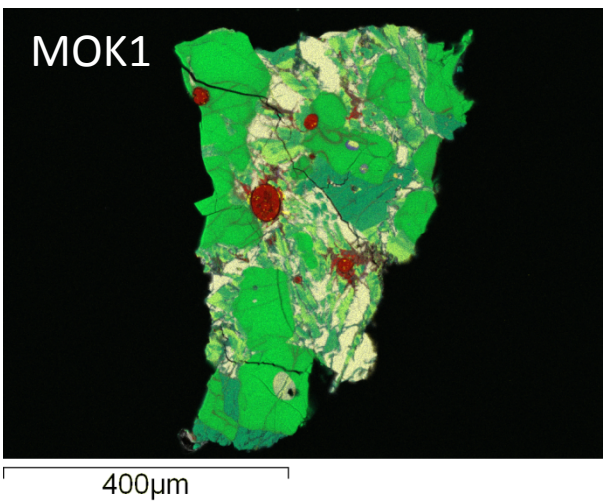
MOK1
400μm

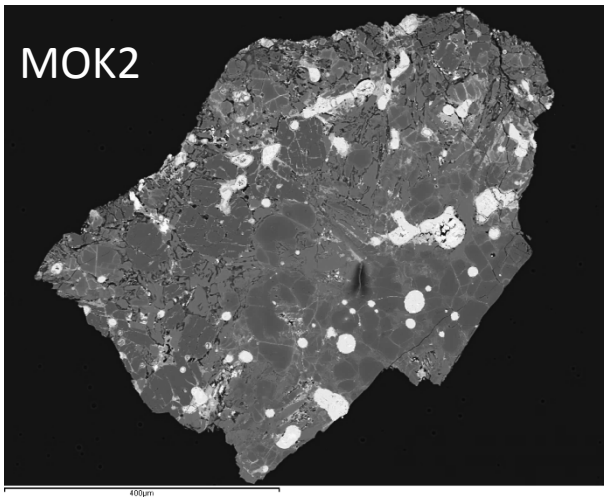
MOK2

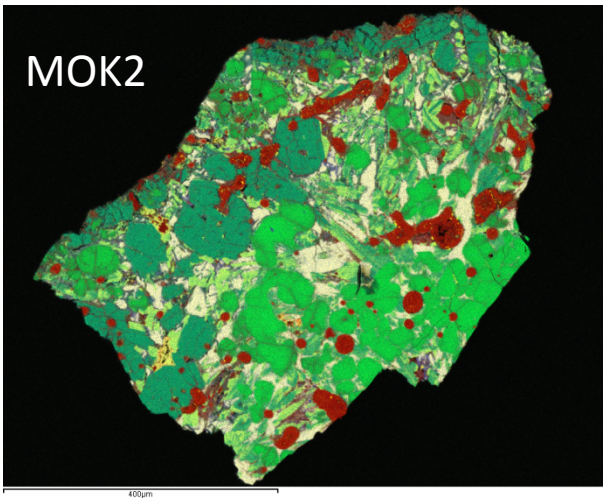
MOK2

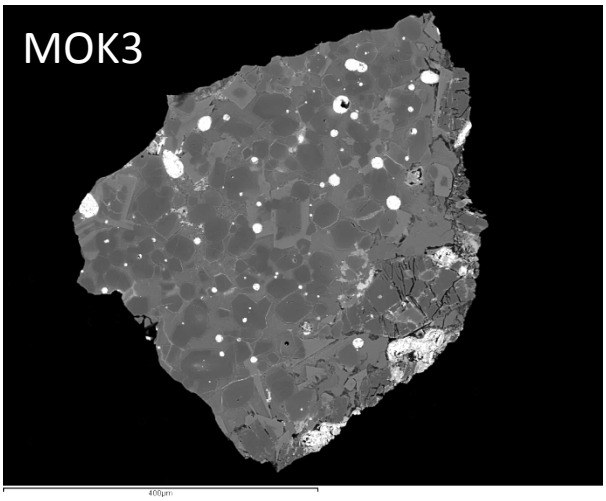
MOK3

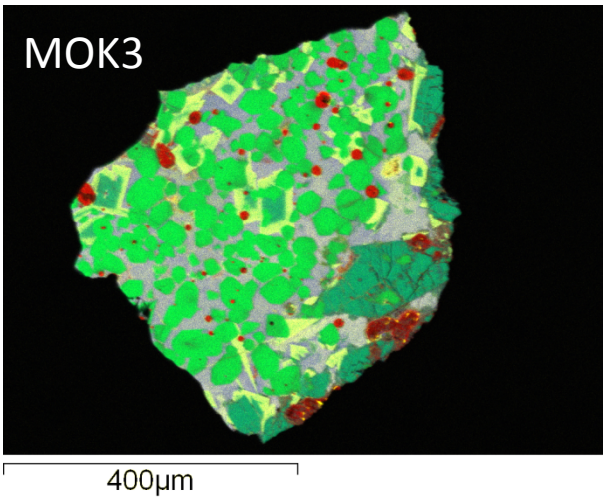
MOK3
400µm

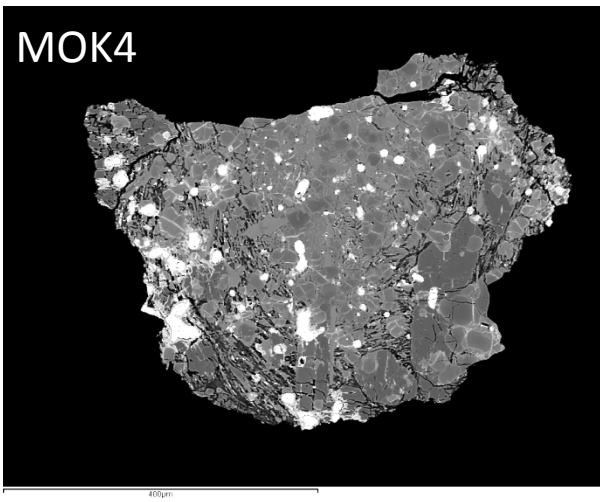
MOK4

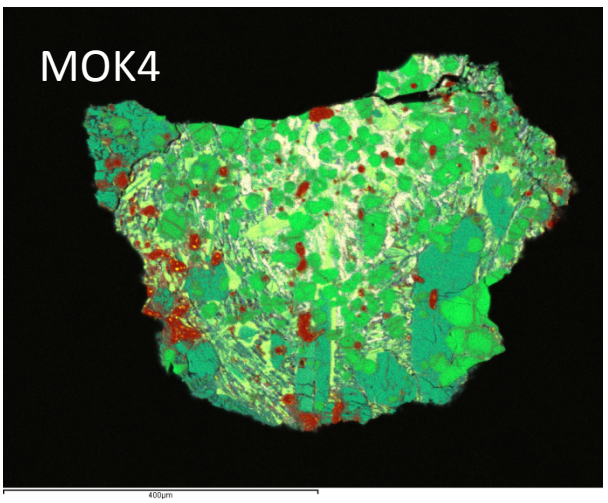
MOK4

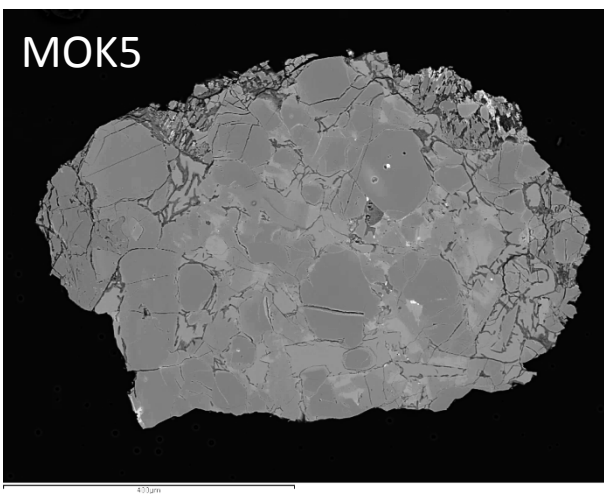
MOK5

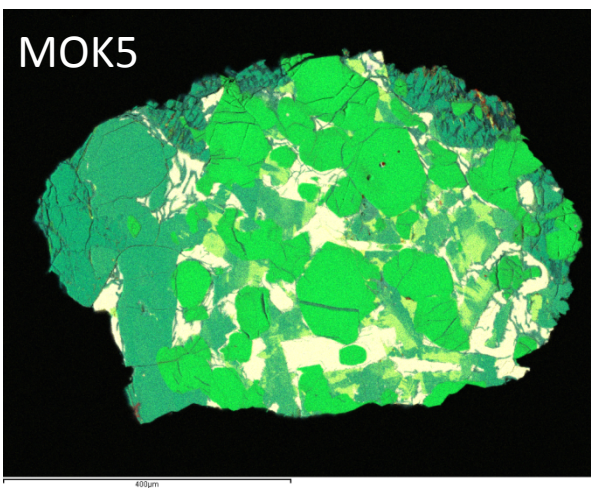
MOK5

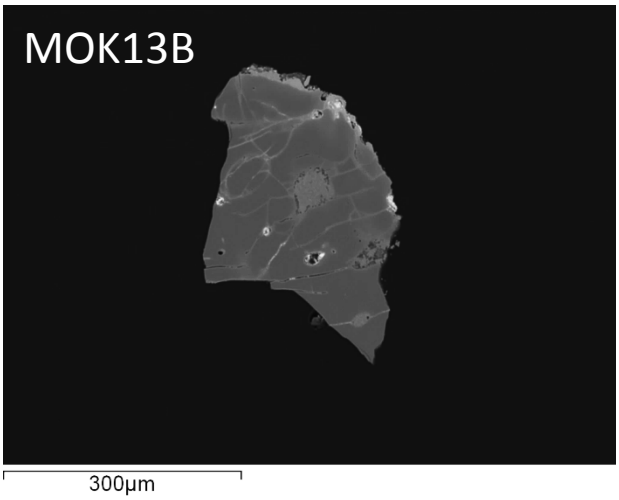
MOK13B
300µm

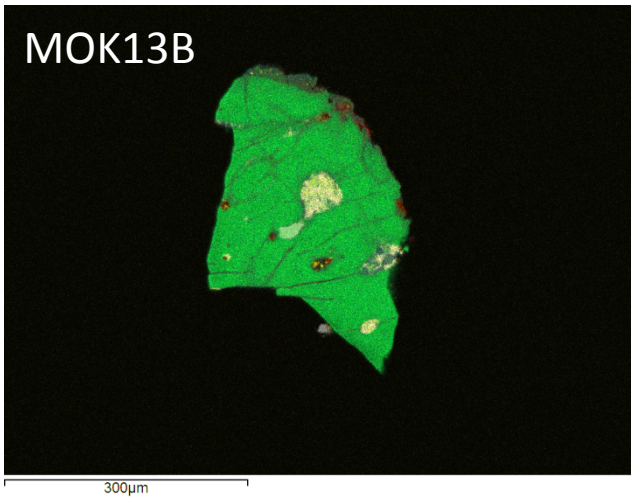
MOK13B
300µm

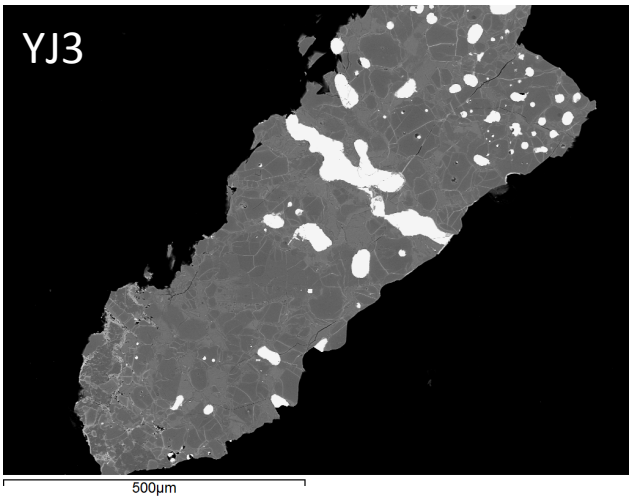
YJ3
500µm

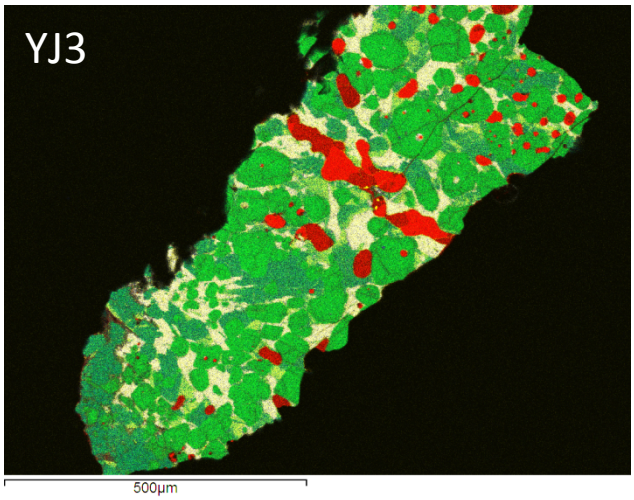
YJ3
500µm

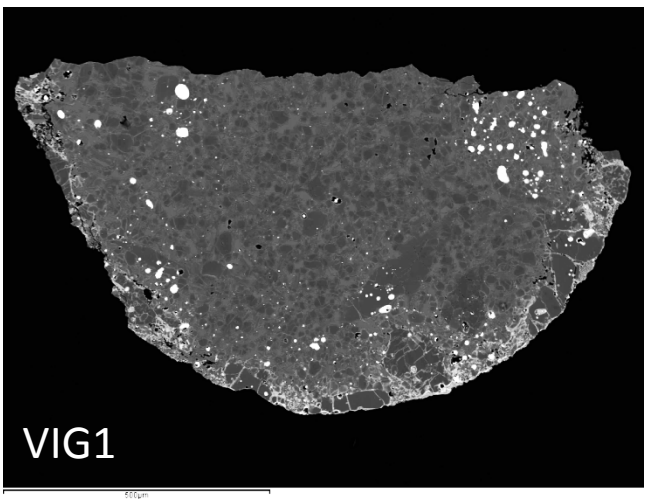
VIG1

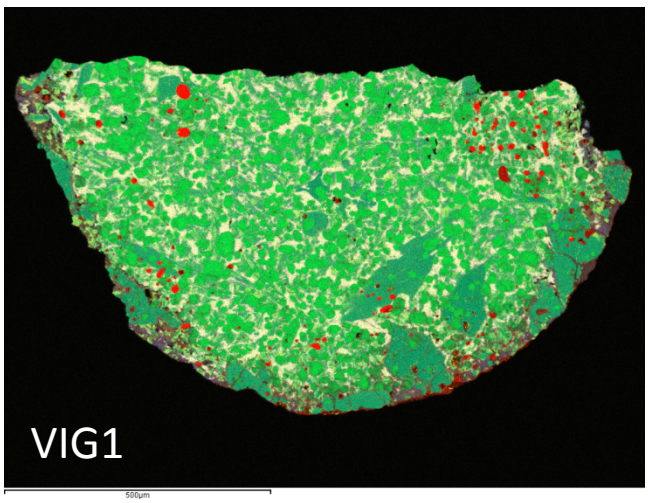
VIG1

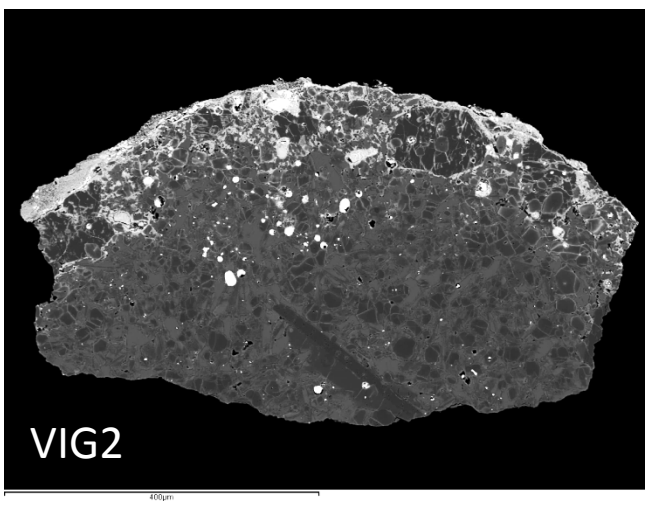
VIG2

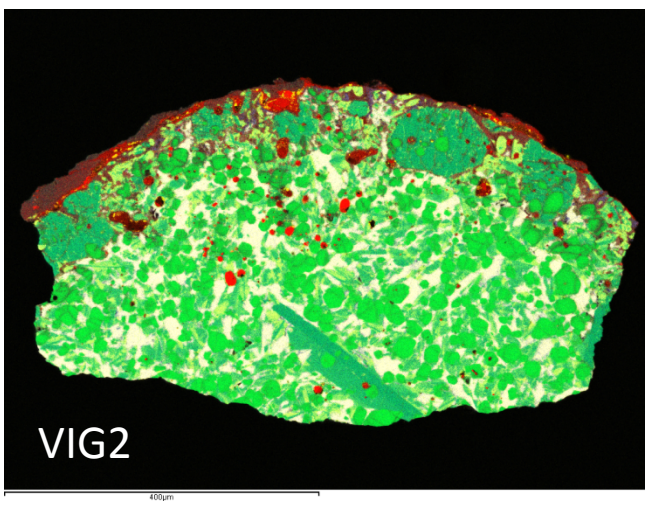
VIG2

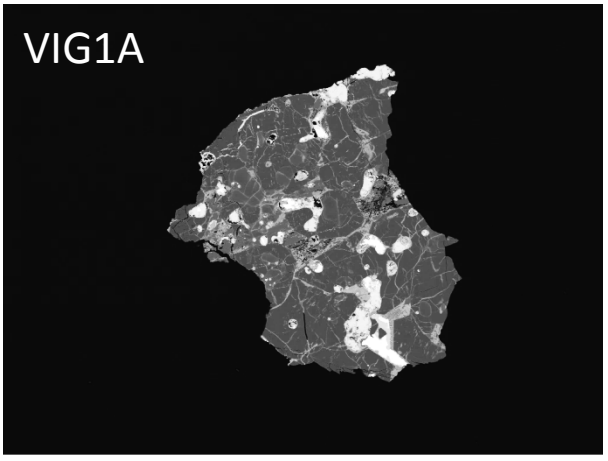
VIG1A
700µm

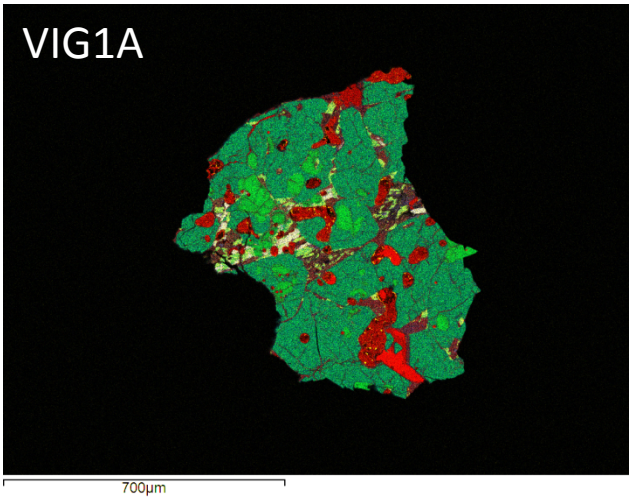
VIG1A
700µm

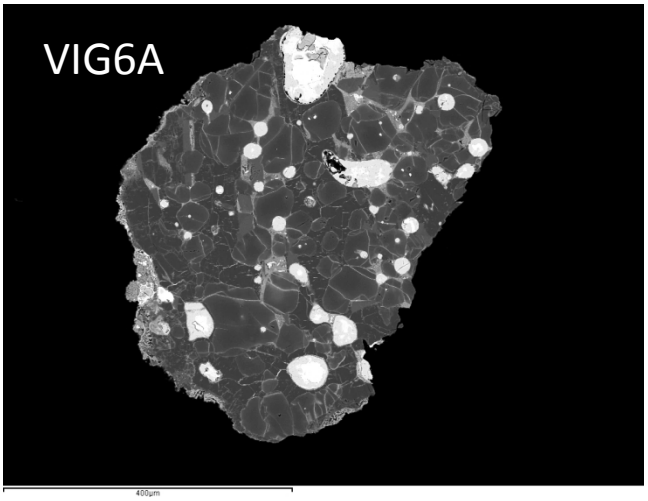
VIG6A

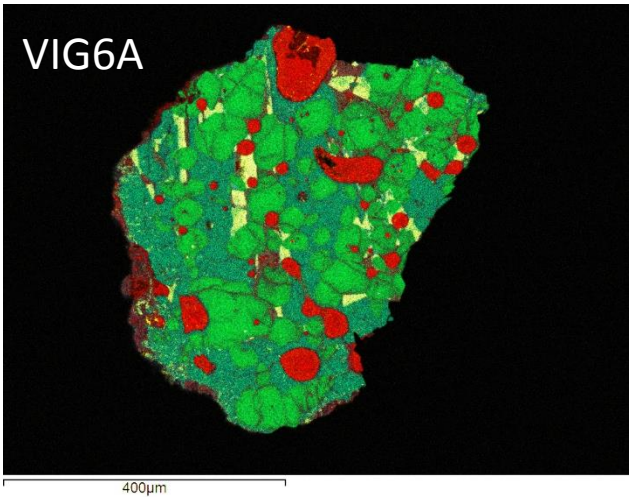
VIG6A
400µm

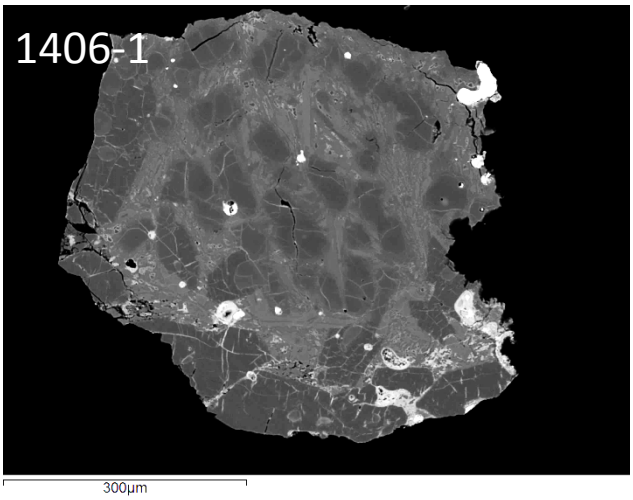
1406-1
300µm

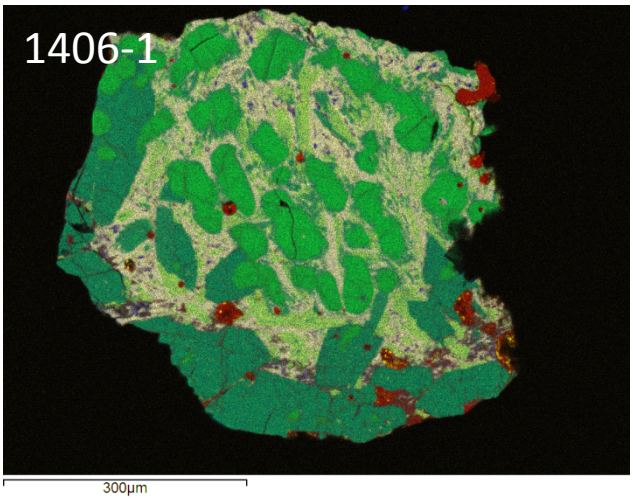
1406-1
300µm

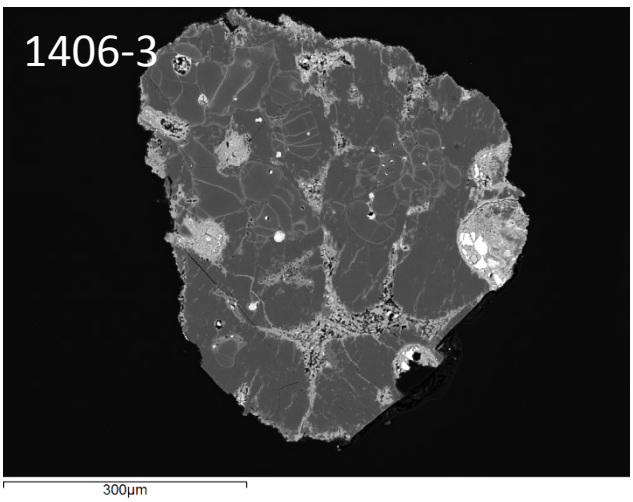
1406-3
300µm

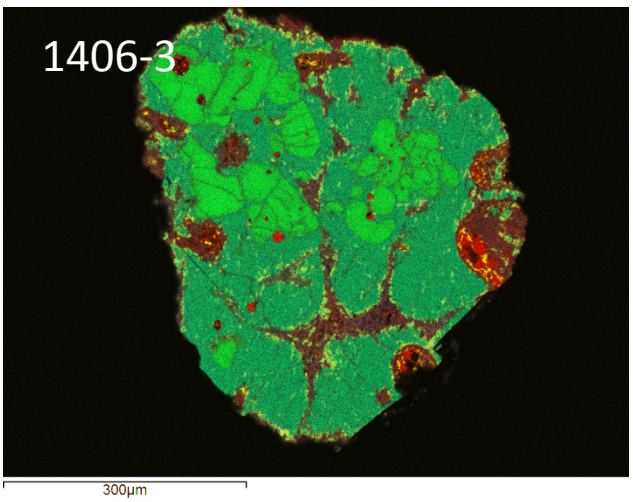
1406-3
300µm

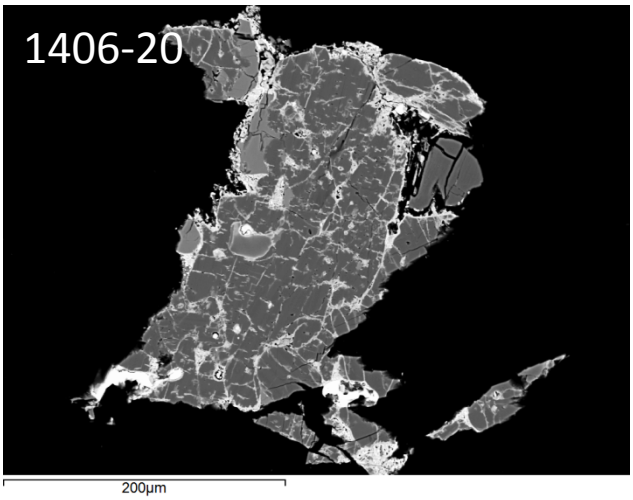
1406-20
200µm

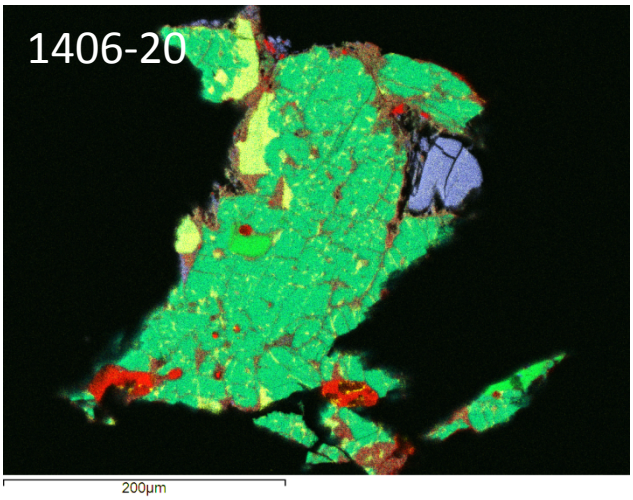
1406-20
200µm

Electronic Annex 2. Typical electron microprobe analyses

Typical olivine analyses

Chondrule	YJ3	YJ3	YJ3	YJ3	YJ4	YJ4	YJ4	YJ4	YJ5	YJ5	YJ5	YJ5	YJ5	YJ5	YJ5
	1 / 2 .	1 / 7 .	1 / 10 .	1 / 27 .	1 / 2 .	1 / 6 .	1 / 7 .	1 / 8 .	1 / 2 .	1 / 3 .	1 / 7 .	1 / 8 .	1 / 9 .	1 / 10 .	1 / 13 .
MgO	52.07	51.75	51.02	52.16	54.17	54.22	54.53	54.56	45.64	48.51	49.38	40.89	51.70	51.04	45.32
Al2O3	bd	0.03	0.10	bd	0.07	0.16	0.05	0.05	0.05	0.04	0.04	0.03	bd	bd	0.07
SiO2	41.30	41.43	40.79	41.57	41.83	42.36	42.45	42.39	40.11	40.77	41.02	38.93	41.71	41.26	40.00
CaO	0.26	0.17	0.18	0.21	0.28	0.44	0.25	0.27	0.18	0.12	bd	0.20	0.22	0.22	0.11
TiO2	bd	bd	0.10	bd	0.08	bd	bd	bd	bd	bd	bd	bd	bd	bd	bd
Cr2O3	bd	0.08	0.64	bd	0.16	bd	0.13	0.14	0.13	0.10	0.13	0.08	bd	bd	0.23
MnO	0.18	0.19	0.15	0.18	bd	bd	bd	bd	bd	bd	0.12	0.12	0.12	0.12	0.12
FeO	5.63	5.95	6.60	5.87	2.79	2.86	2.98	3.06	13.75	9.78	9.38	20.03	6.40	7.79	14.41
TOTAL	**99.43**	**99.60**	**99.58**	**99.99**	**99.37**	**100.03**	**100.39**	**100.47**	**99.86**	**99.32**	**100.06**	**100.29**	**100.15**	**100.42**	**100.26**
Fo [Avg]	**94.09**	**93.61**	**92.86**	**93.83**	**96.82**	**96.49**	**96.57**	**96.55**	**85.29**	**89.50**	**90.14**	**78.32**	**93.15**	**92.05**	**84.64**

Typical Pyroxene Analyses

Chondrule	YJ3	YJ3	YJ5	YJ5	YJ6a	YJ6a	YJ6a	YJ6a	YJ8	YJ8	YJ9	YJ9	YJ9	MOK13B	1406-1
	1 / 12 .	1 / 15 .	1 / 19 .	1 / 18 .	1 / 29 .	1 / 6 .	1 / 14 .	1 / 4 .	1 / 23 .	1 / 4 .	1 / 11 .	1 / 13 .	1 / 14 .	1 / 2 .	1 / 3 .
MgO	35.00	34.27	38.72	37.28	37.42	36.92	20.78	19.45	38.05	27.00	37.72	36.44	22.75	19.49	36.51
Al2O3	1.36	2.23	0.77	1.06	1.53	1.05	2.79	2.53	1.09	2.80	1.21	1.76	3.11	6.05	1.42
SiO2	57.57	56.68	59.46	58.28	58.69	58.59	54.00	53.97	58.55	54.37	58.88	58.00	53.80	53.62	57.76
CaO	2.39	2.55	0.54	0.91	0.73	1.12	20.24	21.92	0.70	11.00	0.72	1.29	17.10	20.24	1.56
TiO2	0.24	0.37	0.20	0.15	0.30	0.20	0.97	0.90	0.25	0.96	0.15	0.32	0.91	1.34	0.25
Cr2O3	1.16	1.32	0.44	0.53	0.66	0.49	0.54	0.46	0.46	0.67	0.45	0.56	0.65	0.32	0.74
MnO	0.22	0.19	bd	bd	bd	bd	0.18	0.16	bd	0.15	bd	bd	0.21	bd	0.13
FeO	2.07	2.07	0.75	1.91	1.03	1.59	0.81	0.95	0.85	2.56	1.06	1.03	0.91	0.45	2.16
TOTAL	**100.01**	**99.68**	**100.88**	**100.13**	**100.35**	**99.95**	**100.30**	**100.34**	**99.94**	**99.51**	**100.19**	**99.40**	**99.43**	**101.50**	**100.53**

Typical Plagioclase Analyses

Chondrule	YJ6	YJ6	YJ6	YJ6	YJ6	YJ8	YJ8	YJ9	YJ9	YJ9	YJ9	MOK13B	VIG1A	VIG1A	YJ10
	1 / 1 .	**1 / 3 .**	**1 / 5 .**	**1 / 8 .**	**1 / 9 .**	**1 / 1 .**	**1 / 6 .**	**1 / 5 .**	**1 / 6 .**	**1 / 9 .**	**1 / 11 .**	**1 / 12 .**	**1 / 7 .**	**1 / 3 .**	**1 / 1 .**
SiO2	45.73	45.97	45.68	46.12	45.76	45.91	46.13	47.49	47.85	47.44	47.15	44.83	47.59	48.11	43.70
Al2O3	32.87	32.13	32.56	32.41	32.10	33.29	32.95	32.02	31.46	31.72	32.26	33.08	32.14	31.76	34.75
FeO	0.62	0.88	0.53	0.84	0.73	0.96	1.22	0.17	0.27	0.38	0.21	0.68	1.24	1.44	0.19
MgO	0.43	0.49	0.43	0.43	0.49	0.52	0.47	0.90	0.98	0.91	0.87	0.49	0.25	0.26	0.22
CaO	18.05	18.41	18.77	18.31	18.47	17.81	16.90	17.79	17.61	17.75	17.80	19.26	16.78	16.75	20.27
K2O	bd	bd	bd	bd	bd	bd	bd	bd	bd	bd	bd	bd	0.15	bd	bd
Na2O	1.69	1.31	1.28	1.39	1.62	1.51	1.85	1.55	1.71	1.65	1.47	0.72	2.16	2.31	0.16
TiO2	bd	bd	bd	bd	bd	bd	bd	bd	bd	bd	bd	0.09	bd	bd	bd
TOTAL	**99.38**	**99.18**	**99.26**	**99.50**	**99.17**	**100.00**	**99.52**	**99.92**	**99.87**	**99.84**	**99.74**	**99.14**	**100.30**	**100.62**	**99.28**
An	**85.60**	**85.60**	**87.10**	**85.50**	**85.20**	**86.00**	**83.40**	**82.30**	**80.50**	**81.60**	**83.20**	**90.70**	**79.70**	**78.20**	**96.80**

Data are in weight %
bd = below detection.

YJ5	YJ6	YJ6	YJ6	YJ6	YJ6	YJ7	YJ7	YJ7	YJ7	YJ8	YJ8	YJ8	YJ9	YJ9	MOK13B	MOK13B
1 / 14 .	1 / 2 .	1 / 6 .	1 / 9 .	1 / 11 .	1 / 4 .	1 / 4 .	1 / 8 .	1 / 9 .	1 / 10 .	1 / 1 .	1 / 2 .	1 / 9 .	1 / 9 .	1 / 2 .	1 / 4 .	1 / 7 .
36.14	56.07	55.30	52.34	53.00	55.76	42.48	38.00	36.34	34.33	51.63	55.96	47.51	56.81	54.53	53.82	54.95
0.15	0.19	0.15	0.05	0.13	0.11	bd	bd	0.03	bd	bd	bd	0.25	0.22	0.14	0.12	0.11
37.26	42.68	42.42	41.97	41.90	42.68	39.67	38.50	38.22	37.50	41.38	42.59	40.05	42.63	42.19	42.48	42.74
0.18	0.35	0.37	0.23	0.24	0.32	0.09	0.12	0.11	0.14	0.22	0.23	0.20	0.37	0.27	0.40	0.35
bd	bd	0.11	bd	0.10	bd	bd	bd	bd	bd	bd	bd	bd	bd	bd	0.11	0.15
0.46	0.23	0.26	0.12	0.19	0.18	0.15	0.08	0.08	0.10	0.22	0.39	0.73	0.11	0.45	0.18	0.18
0.14	bd	bd	bd	bd	bd	0.21	0.27	0.26	0.26	0.20	0.14	0.10	bd	0.14	bd	bd
25.78	0.88	1.73	5.62	4.61	1.12	18.02	23.76	25.65	27.73	7.14	1.07	11.77	0.37	2.43	4.40	2.84
100.09	**100.39**	**100.35**	**100.33**	**100.14**	**100.18**	**100.63**	**100.72**	**100.67**	**100.07**	**100.79**	**100.38**	**100.62**	**100.51**	**100.15**	**101.50**	**101.30**
71.39	**98.55**	**97.68**	**93.86**	**94.87**	**98.29**	**80.50**	**73.88**	**71.44**	**68.67**	**92.67**	**98.45**	**87.55**	**99.29**	**96.92**	**95.06**	**96.58**

1406-3	1406-3	1406-3	1406-20	VIG1A	VIG6A	YJ10	YJ10	MOK1	MOK2	MOK2	MOK3	MOK3	MOK3	MOK4	MOK4	MOK4
1 / 19 .	1 / 15 .	1 / 28 .	1 / 15 .	1 / 27 .	1 / 21 .	1 / 6 .	1 / 2 .	1 / 10 .	1 / 6 .	1 / 15 .	1 / 50 .	1 / 5 .	1 / 8 .	1 / 8 .	1 / 2 .	1 / 1 .
38.33	36.79	31.33	22.14	22.71	37.63	15.38	12.13	34.90	38.26	38.11	38.19	38.02	35.78	37.36	36.43	35.91
0.00	0.00	0.00	1.33	3.14	0.80	7.90	16.52	2.01	1.37	1.02	1.41	1.18	2.48	1.78	1.99	1.99
59.50	58.16	58.04	54.68	54.22	58.78	49.25	44.19	56.22	57.96	57.65	57.98	57.87	55.07	57.86	57.69	57.37
0.37	1.74	6.62	18.77	16.22	0.50	24.82	24.85	3.55	0.61	0.49	0.52	0.55	1.79	0.68	2.17	2.53
0.23	0.11	0.10	0.68	0.57	0.18	2.44	1.80	0.33	0.42	0.27	0.29	0.22	0.45	0.31	0.39	0.35
0.71	0.60	0.59	0.84	0.73	0.49	0.37	bd	0.90	0.36	0.32	0.59	0.67	0.89	0.63	0.84	0.82
bd	bd	bd	0.41	0.27	bd	bd	bd	0.16	bd	0.06	0.12	0.16	0.22	bd	0.14	0.16
1.13	3.38	2.83	1.02	2.30	2.11	0.28	0.38	0.65	0.74	2.34	0.63	0.64	2.67	1.71	0.70	0.79
100.27	**100.79**	**99.51**	**99.87**	**100.16**	**100.49**	**100.44**	**99.87**	**98.72**	**99.72**	**100.26**	**99.72**	**99.31**	**99.34**	**100.33**	**100.35**	**99.92**

YJ10	YJ10	YJ10	YJ10	YJ10	YJ10	MOK1	MOK1	MOK2	MOK2	VIG2	VIG2	VIG2	VIG2	VIG2
1 / 5 .	**1 / 11 .**	**1 / 1 .**	**1 / 2 .**	**1 / 3 .**	**1 / 4 .**	**1 / 1 .**	**1 / 6 .**	**1 / 1 .**	**1 / 3 .**	**1 / 5 .**	**1 / 6 .**	**1 / 11 .**	**1 / 3 .**	**1 / 1 .**
43.30	43.61	43.35	43.18	43.04	43.38	46.27	46.94	47.32	47.34	46.17	46.20	45.94	45.78	46.41
35.07	34.56	35.84	35.98	35.91	35.60	32.17	32.48	31.52	31.55	32.04	32.14	32.32	32.72	32.23
0.28	0.40	0.18	0.15	0.20	0.26	1.02	0.36	0.98	0.78	1.04	1.05	1.14	1.21	1.12
0.07	0.11	0.10	0.05	0.07	0.09	0.26	0.55	0.30	0.34	0.54	0.49	0.44	0.32	0.46
20.12	20.03	19.86	20.15	20.07	19.87	17.52	17.49	16.63	16.79	17.49	17.32	17.66	17.78	17.30
bd	bd	bd	bd	bd	bd	bd	bd	bd	bd	bd	bd	bd	bd	bd
0.19	0.26	0.15	0.07	0.08	0.18	1.82	1.92	2.27	2.18	1.78	1.84	1.73	1.74	1.94
bd	0.09	bd	bd	bd	bd	bd	bd	0.03	0.05	bd	bd	bd	bd	bd
99.02	**99.05**	**99.48**	**99.58**	**99.37**	**99.37**	**99.06**	**99.74**	**99.05**	**99.03**	**99.06**	**99.04**	**99.23**	**99.55**	**99.46**
97.50	**96.20**	**98.20**	**99.10**	**99.10**	**97.80**	**83.00**	**82.30**	**78.80**	**79.20**	**83.00**	**82.80**	**84.00**	**84.90**	**82.40**

MOK13B	**MOK13B**	**1406-1**	**1406-1**	**1406-3**	**1406-20**	**1406-20**	**VIG1A**	**VIG6A**	**YJ10**
1 / 11 .	1 / 12 .	1 / 1 .	1 / 3 .	1 / 6 .	1 / 3 .	1 / 2 .	1 / 11 .	1 / 1 .	1 / 11 .
56.51	56.25	55.56	55.59	48.21	48.10	51.08	43.20	48.80	36.79
0.22	0.21	bd	bd	0.14	0.08	0.06	bd	0.14	0.64
42.97	42.91	42.93	43.03	40.18	41.03	41.86	38.08	39.99	36.52
0.58	0.63	0.25	0.21	0.17	0.22	0.17	0.23	0.18	0.67
bd	bd	bd	bd	bd	bd	bd	bd	bd	bd
0.09	0.09	bd	0.13	0.91	0.15	0.09	1.57	0.23	0.17
bd	bd	0.23	0.22	bd	0.18	0.15	0.12	0.11	0.21
0.32	0.29	2.48	2.56	10.49	10.91	7.37	16.43	11.10	24.06
100.69	**100.37**	**101.45**	**101.73**	**100.11**	**100.68**	**100.78**	**99.62**	**100.73**	**99.06**
98.94	**98.87**	**97.16**	**97.04**	**88.82**	**88.25**	**92.01**	**82.36**	**88.94**	**73.11**

MOK5	**MOK5**	**MOK5**	**VIG1**	**VIG1**	**VIG2**	**VIG2**
1 / 10 .	1 / 2 .	1 / 1 .	1 / 17 .	1 / 14 .	1 / 8 .	1 / 3 .
37.29	34.73	33.43	38.29	37.12	31.12	29.35
0.76	1.09	2.04	0.86	1.65	3.56	3.32
58.10	57.12	55.90	58.34	57.63	55.25	55.53
0.41	2.07	2.54	0.81	1.97	6.70	9.43
0.10	0.14	0.34	0.22	0.32	0.92	0.95
0.71	1.10	1.43	0.54	0.62	0.88	0.81
bd	0.37	0.68	bd	0.14	0.29	0.23
2.16	2.96	3.64	bd	0.70	1.41	0.59
99.53	**99.58**	**100.00**	**99.06**	**100.15**	**100.12**	**100.21**